Some aspects of the South American monsoon variability

Alice M. Grimm
Department of Physics, Federal University of Paraná, Curitiba, Paraná, Brazil
grimm@fisica.ufpr.br

ICTP 2016: Towards Improved Monsoon Simulations

Annual cycles of precipitation

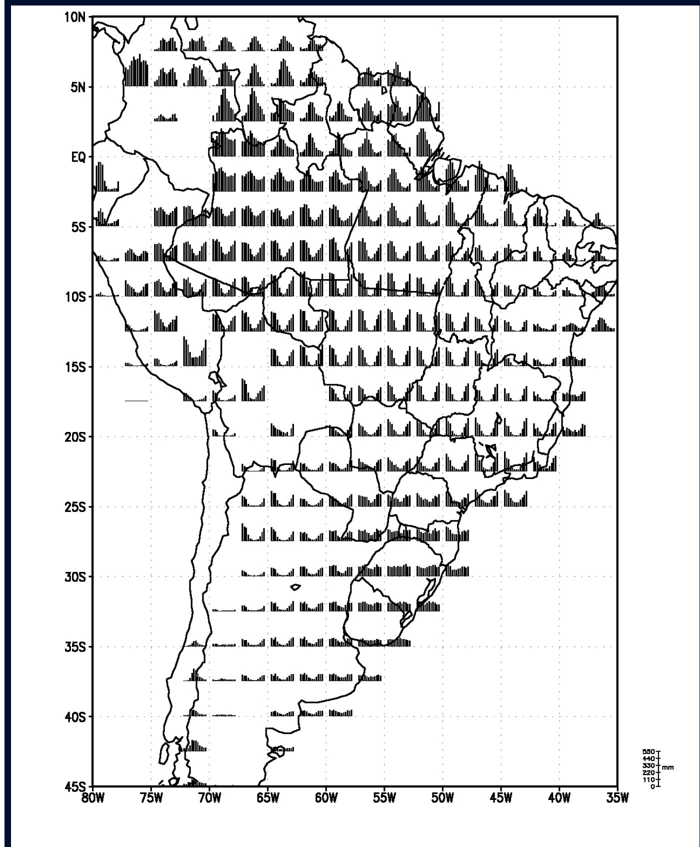

From Grimm 2011

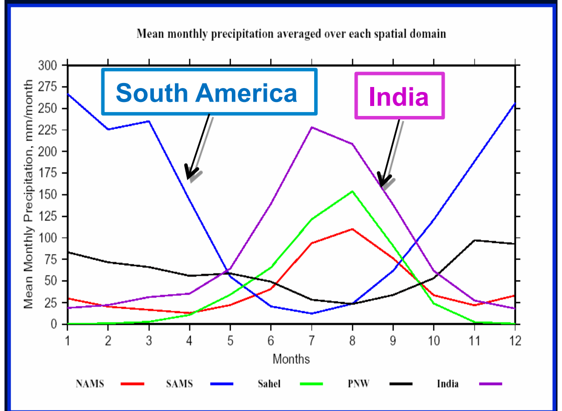

From Vera, Higgins, Amador et al. 2006

General features of the SAMS

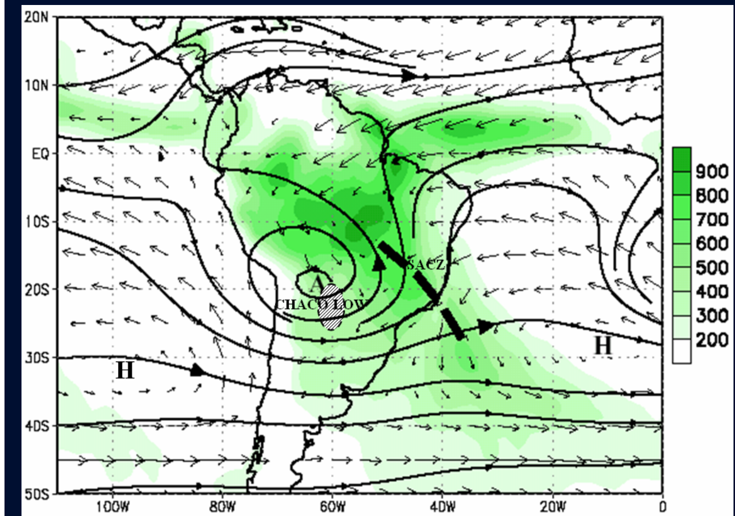

Courtesy of V. Kouski

Chaco Low – SACZ - Bolivian High - Nordeste Low – SALLJ (DJF)

- In austral summer, a thermal low-pressure system intensifies over the Chaco region.
- The tropical northeasterly trade winds are enhanced
- Cross-equatorial flow penetrates SA, becomes northwesterly at the Andes foothills, is channeled southward, and turns clockwise around the Chaco low.
- Low-level wind and moisture convergence associated with the interaction between the continental low, the South Atlantic high and the northwesterly winds result in enhanced precipitation in the Amazon, and Central and Southeast Brazil.

Evolution of the SAMS

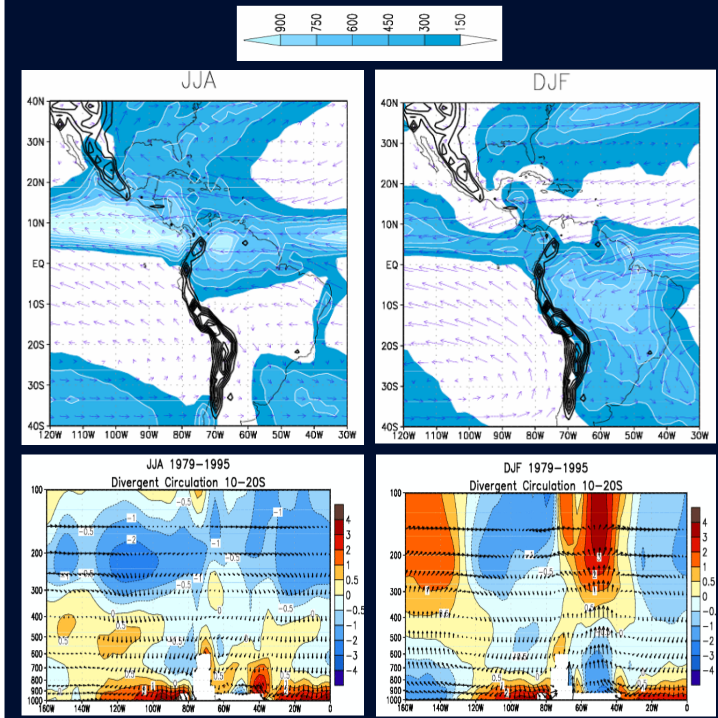

From Marengo, Liebmann, Grimm et al. 2012

- The onset of the convection is controlled by changes in the thermodynamic structure related to the moistening of the boundary layer and the lowering of temperature at its top.
- They are brought about by changes in large-scale circulation that enhance low-level moisture convergence into the region, particularly a southward enhancement of the cross-equatorial flow.
- The land surface warming increases the gradient of land-ocean temperature and drives the seasonal changes of circulation.
- Changes of circulations are largely controlled by the SST in the adjacent oceans and southern Amazon.

Evolution of the SAMS

Courtesy of V. Kouski

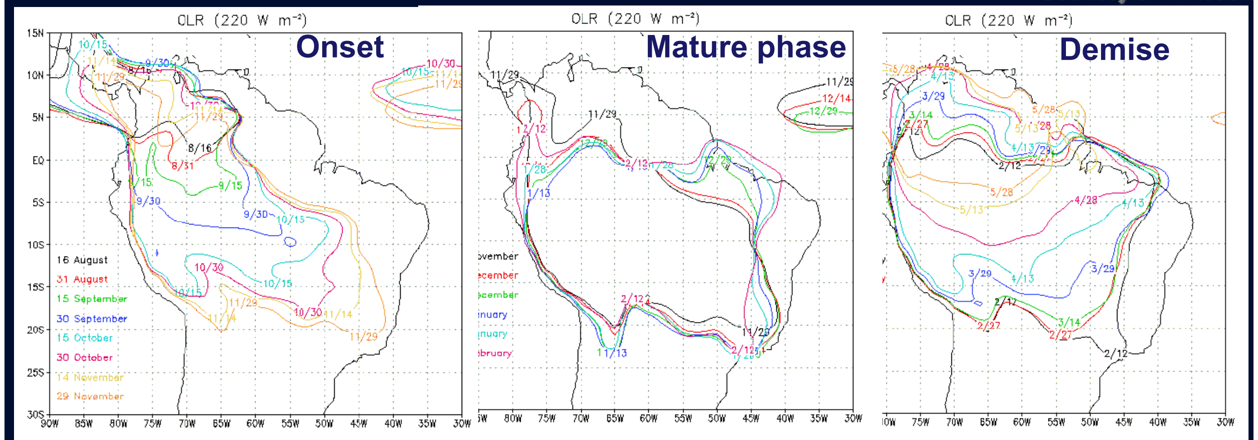

❑Although the large-scale circulation patterns associated with the SAMS are driven by large-scale distributions of sensible and latent heating, with the Andes Mountains and other orographic features playing an important role in the dynamics of the monsoon system, there are numerous synoptic and mesoscale features embedded within these large-scale circulation patterns. These features are responsible for the day-to-day weather and high impact rainfall events. Extreme rainfall events that affect the most populous regions in South America are most frequent in the summer monsoon season.

Contribution of synoptic and intraseasonal timescales to total variance of summer rainfall

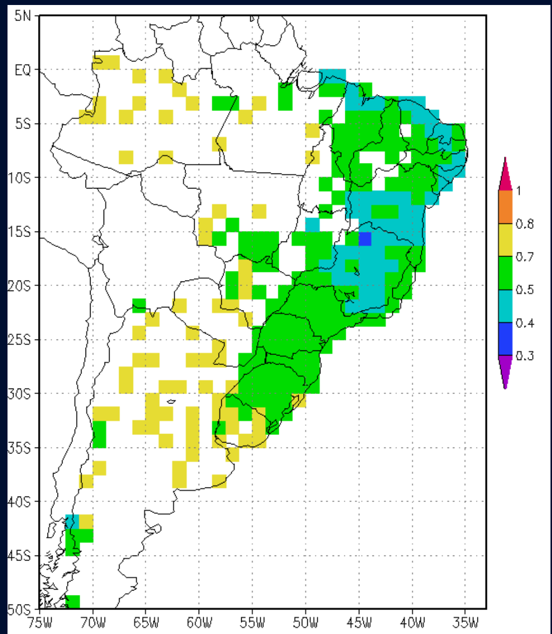

Synoptic variability

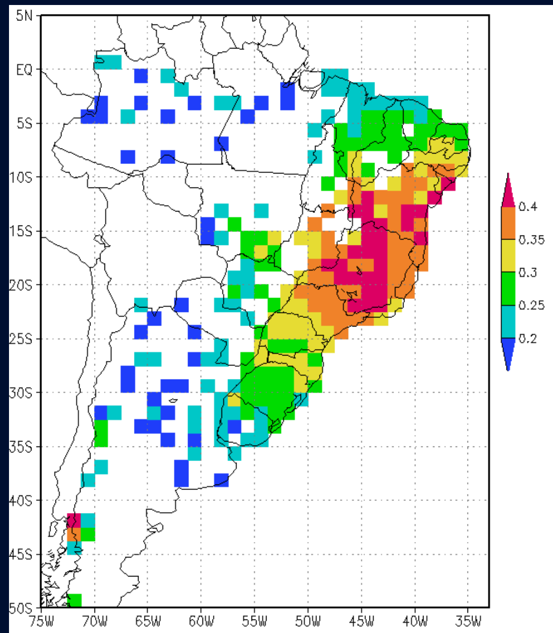

Intraseasonal variability

Ferraz and Grimm 2004

Synoptic Features

During austral summer, the daily precipitation variability over tropical South America results mainly from the combined action of:

- ❑ equatorial trades,
- ❑ easterly tropical disturbances,
- ❑ equatorward incursions of midlatitude synoptic wave systems.

Equatorward incursions of frontal systems

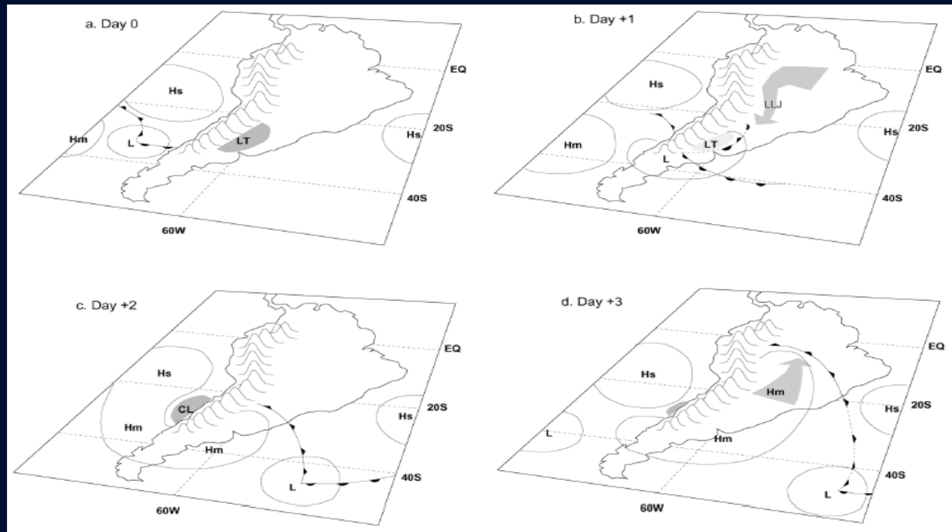

❑ The day-to-day variability of rainfall over subtropical South America and western Amazon basin is largely explained by northward incursions of mid-latitude systems to the east of the Andes, even in summer (Gan and Rao 1994; Vera et al. 2002) . The deep northward intrusion of midlatitude systems is attributed to the dynamical effect of the Andes topography, which plays a significant on the structure and evolution of the synoptic systems that cross South America.

Equatorward incursions of frontal systems

From Garreaud and Wallace 1998

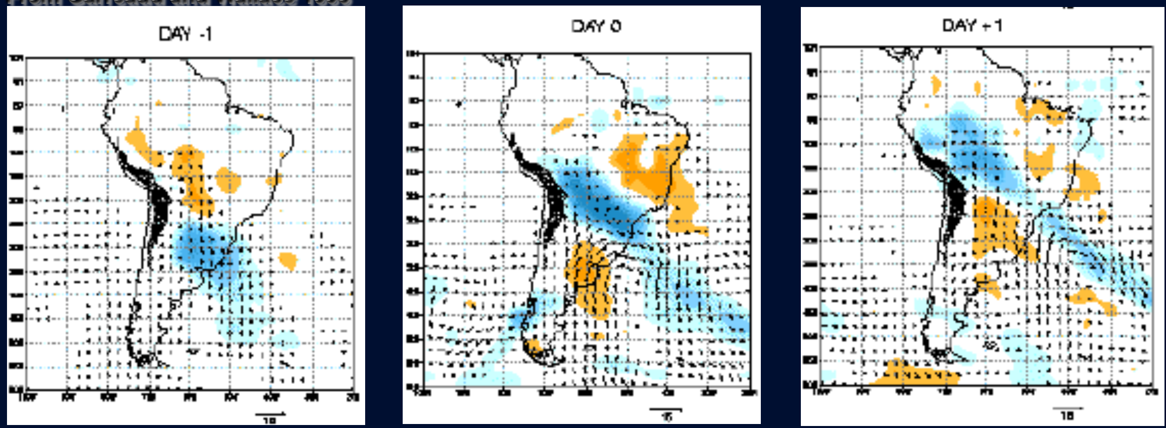

❑ Cold fronts tend to be directed northward to the east of the Andes, fostering the advance of cold air incursions into subtropical/tropical latitudes. In summer there is large impact on the precipitation, through the equatorward propagation (~10 ms^{-1}) of a northwest-southeast oriented band of enhanced convection ahead of the leading edge of the cool air, which tends to be followed by an area of suppressed convection. This synoptic scale banded structure, which maintains its identity for about 5 days, is the dominant mode of the day-to-day variability of deep convection, contributing with ~25% of summer precipitation in the central Amazonia and ~50% over subtropical South America. These bands influence convection in the SACZ.

Frontal systems influence on tropical convection

Three types of frontal system influence on tropical convection:

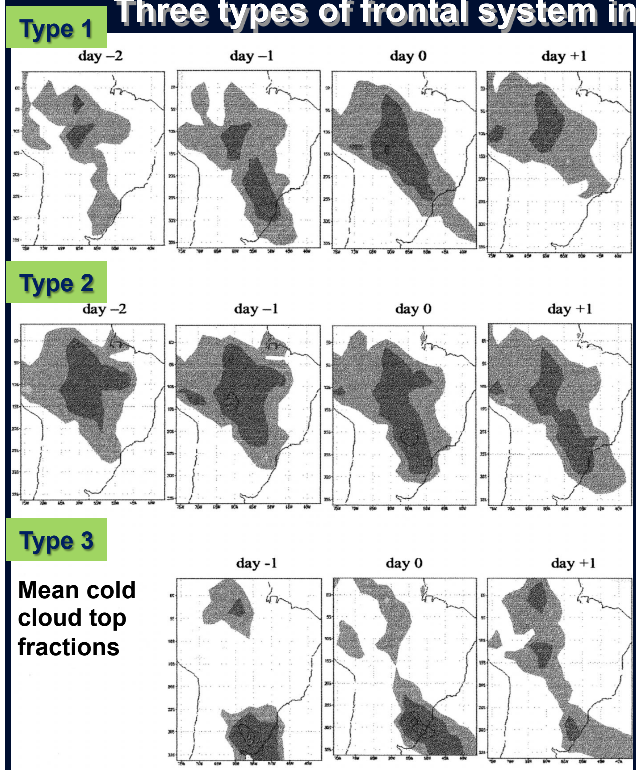

Siqueira and Machado 2004; Siqueira et al. 2005

- ❑ **Type 1** - frequent in austral summer, is characterized by the penetration of a cold front in subtropical South America that interacts with tropical convection and moves with it into lower tropical latitudes.
- ❑ **Type 2** - also more frequent in austral summer, is characterized by Amazon convection and southward enhancement of convection in a quasi-stationary northwest–southeast band by the passage of a cold front in the subtropics. When this pattern remains longer than 4 days, it often characterizes the SACZ.
- ❑ **Type 3** - more frequent in austral winter, is represented by a quasi-stationary cold front in subtropical South America and midlatitudes, without significant interaction with tropical convection.

Mesoscale Features

- There are major regional differences in the structure, intensity, and diurnal cycle of rainfall systems. While the La Plata Basin, in SESA, is particularly dominated by large and intense MCSs (average area: ~5×10^5 km^2; average lifetime: ~12 hours), the rainfall in the Amazon Basin comes partly from smaller MCSs (average area less than 1×10^5 km^2 and shorter lifetime: 3-6 hours) and partly from frequent showers and thunderstorms.
- There are significant differences in horizontal dimensions and vertical development of MCSs for the 3 types of frontal system interaction with tropical convection. For instance, Type 2, often evolving into SACZ, shows larger horizontal extent with weaker vertical development than Type 1.
- MCSs are influenced by mesoscale effects such as jets and other topographically forced circulation and surface atmosphere interactions. The SALLJ is the jet with most extensive influence.
- MCSs are modulated by the diurnal cycle.

Synoptic Variability X SALLJ

❑The SALLJ events are conditioned by synoptic variability, and can be separated into two groups:

❑ (1) events in which the LLJ extends farther south, at least to 25°S,

❑ (2) events in which the jet leading edge is north of this threshold.

LLJ Composites NDJF,
(Marengo et al. 2004)

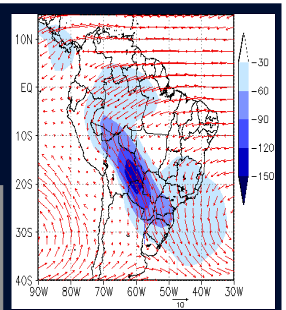

(1) Moisture flux

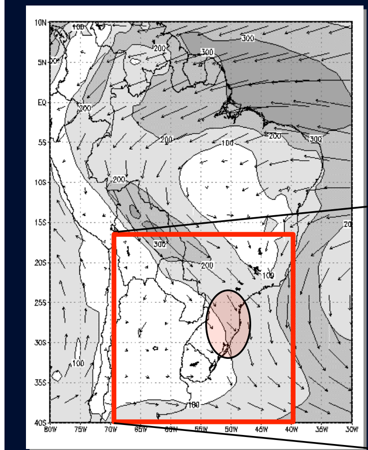

Precipitation

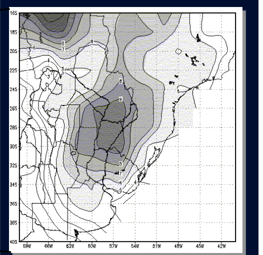

(2) Moisture flux

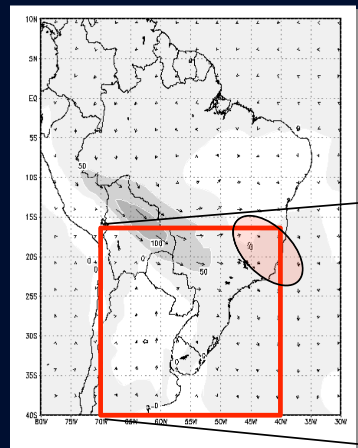

Precipitation

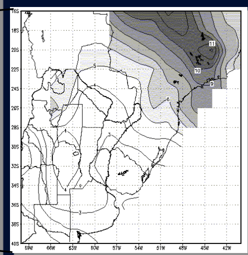

Nicolini et al 2002

Mesoscale Variability

SESA exhibits the most extensive "hot spot" of the most intense thunderstorms on Earth, according to the TRMM data (1 January 1998 - 31 December 2004).

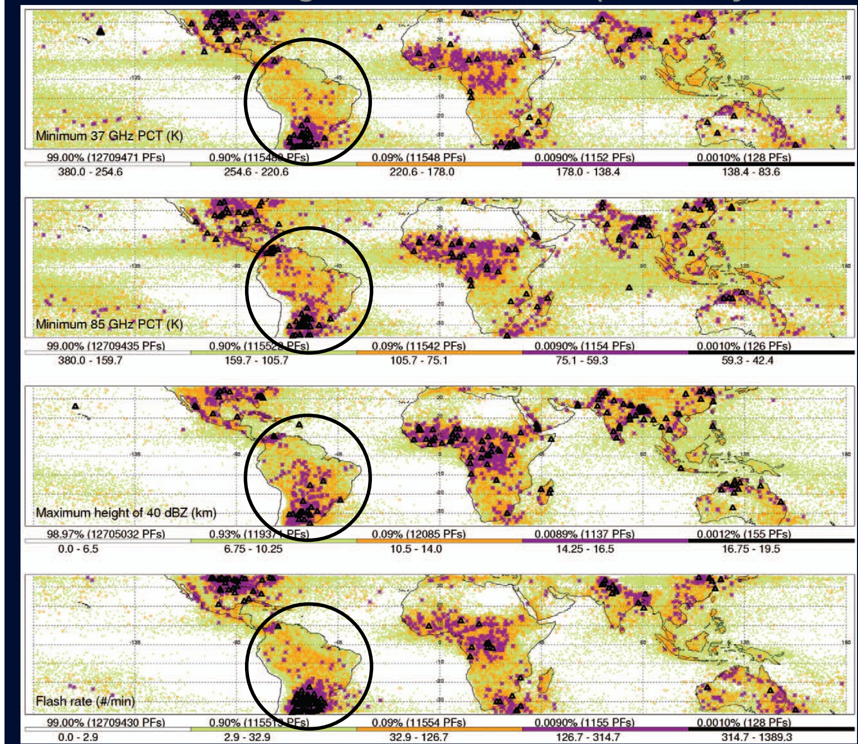

Locations of intense convective events according to different proxies for convection intensity, using the color code matching their rarity. The parameter limits for each category are indicated above each color bar. For example, of the 12.8 million PFs, only about 0.001% (128) have more than 314.7 lightning flashes per minute.

(Zipser et al 2006, BAMS)

Mesoscale Variability

In SESA Mesoscale Convective Complexes (MCCs) occur frequently during October-April.

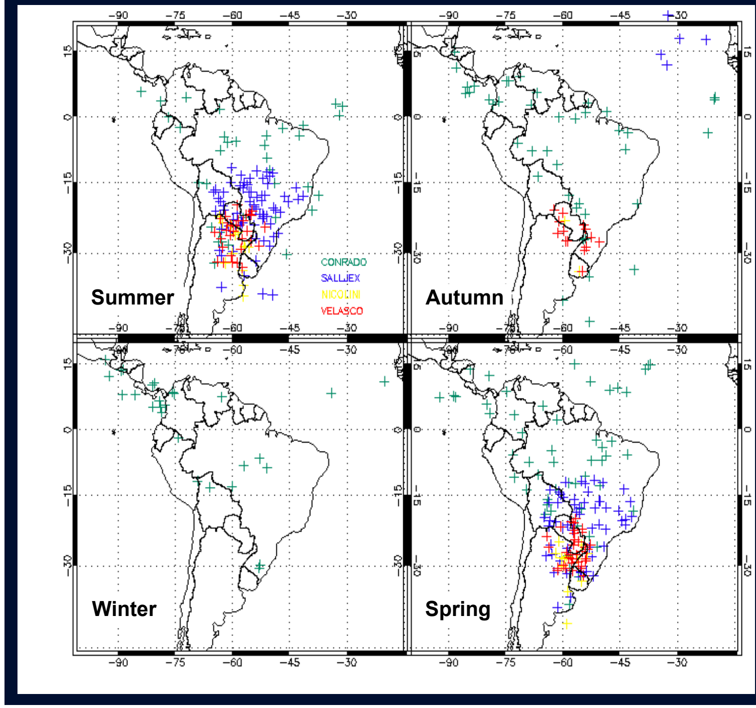

- Average area: ~5×10^5 km^2
- Average lifetime: ~12 hours
- Cycle: preferentially initiate in late afternoon and mature during nighttime.
- Develop east of the Andes, and move preferentially southeastward.
- Intensification related with the subtropical jet and SALLJ.
- More than 80% of MCCs occur during SALLJ events that penetrate farther south.

Compilation of the MCCs location as given by several works (J. C. Conforte)

The Role of Synoptic and Intraseasonal Anomalies in the Life Cycle of Summer Rainfall Extremes over the SACZ

The role of synoptic and intraseasonal anomalies in the life cycle of summer rainfall extremes over South America

Fernando E. Hirata & Alice M. Grimm

Climate Dynamics
Observational, Theoretical and Computational Research on the Climate System

ISSN 0930-7575

Clim Dyn
DOI 10.1007/s00382-015-2751-6

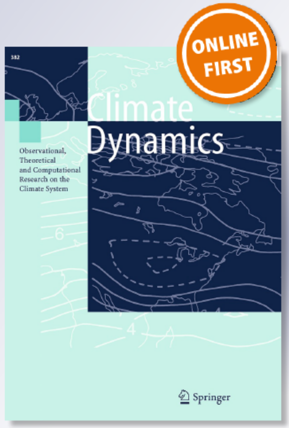

Springer

Clim Dyn
DOI 10.1007/s00382-015-2751-6

CrossMark

The role of synoptic and intraseasonal anomalies in the life cycle of summer rainfall extremes over South America

Fernando E. Hirata[1] · Alice M. Grimm[1]

Received: 4 February 2015 / Accepted: 1 July 2015

Abstract The main goal of this study is to describe the role of synoptic and intraseasonal anomalies during the life cycle of summer rainfall extremes over South America. Eastward-propagating synoptic-scale midlatitude waves are the main drivers of extreme precipitation events south of the Amazon and their interaction with intraseasonal anomalies over South America is important for heavy rainfall over the South Atlantic convergence zone (SACZ) region and the La Plata basin. Madden–Julian Oscillation (MJO) convective activity in the western Pacific (phases 6 and 7) leads 31 out of 81 extremes over the SACZ region by nearly 10 days. The connection between the MJO and rainfall extremes in other regions is less robust. During El Niño seasons extremes are more frequent in the La Plata basin, with decreased importance of intraseasonal anomalies. Precipitation extremes over the La Plata basin tend to be less frequent and also shorter during La Niña summers and, consequently, less hazardous. In the SACZ and the southeastern Brazilian coast, heavy rainfall is also more frequent under El Niño conditions, while La Niña episodes also increase extreme events in the southeastern coast. Extremes over the southeastern coast during El Niños are favored by strong intraseasonal anomalies flanking the subtropical jet, while during La Niñas intraseasonal anomalies are not significant.

Keywords Precipitation · Extreme events · Synoptic disturbances · Intraseasonal variability · South Atlantic convergence zone

✉ Fernando E. Hirata
fernando.endo.hirata@gmail.com

[1] Department of Physics, Universidade Federal do Paraná, Curitiba, Brazil

1 Introduction

Intense precipitation events cause severe floods and mudslides in densely populated regions of South America and affect thousands of people during the warm season (Cavalcanti 2012). Forecasting these extremes is a difficult task. State-of-the-art numerical weather prediction systems and statistical techniques still face many problems when dealing with amplitude, timing and location of rainfall extremes (e.g. Ramírez et al. 2006; Dolif and Nobre 2012). Cavalcanti (2012) reviewed large scale mechanisms and synoptic features associated with extreme precipitation over South America and highlighted the importance of frontal systems and the South Atlantic convergence zone (SACZ) in producing excessive rainfall across the continent. The SACZ is usually defined as a band of deep convection oriented in the northwest–southeast direction and extending from the Amazon to the southwest Atlantic (Fig. 1). Nearly half of heavy rainfall events are caused by frontal systems and the other half, by the SACZ (Lima et al. 2010). Seluchi and Chou (2009) showed that mudslides in the southeastern (SE) Brazilian coast are caused by frontal systems or the SACZ.

Over the La Plata basin, Zipser et al. (2006) identified some of the most intense thurderstorms in the world. Large mesoscale convective systems are frequent during the warm season over the basin (Pereira et al. 2010). A northerly low-level jet over Paraguay and a continental thermal low over northern Argentina are usually associated with heavy rainfall over southern Brazil (Teixeira and Satyamurty 2007). Intense precipitation over the La Plata basin is associated with a midlatitude wave in the upper levels and southward moisture flux from the Amazon, while events over the core of the South American monsoon region (which includes the SACZ) are linked to similar, long-lasting patterns and an eastward shift of the low level jet (Silva and Berbery 2006).

Published online: 14 July 2015

Methods

- Data used: The CPC Unified Gauge-Based Analysis of Global Daily Precipitation dataset at 0.5o horizontal resolution, and NCEP reanalysis data, at 2.5o horizontal resolution, are used to define precipitation extremes and to characterize their synoptic evolution from 1979 to 2013.
- An extreme precipitation event is defined whenever the area-averaged rainfall rate exceeds the 95th percentile for at least one day (~17 mm/day).
- Anomaly composites of several atmospheric fields, from 5 days before to the day of maximum rainfall, are calculated and the significance is assessed.
- Computation of the climatological zonal stretching deformation (zonal variation of the summer climatological zonal wind, $\partial\bar{U}/\partial x$) at 200 hPa, which is related to the longitudinal (zonal) wavenumber of synoptic Rossby waves propagating eastward and wave energy density by Webster and Chang (1988). Negative zonal stretching deformation increases the longitudinal wavenumber, which leads to a reduction of the longitudinal wave speed and increases wave energy density (wave accumulation). This results in intense convective activity that forms the diagonal cloud band characteristic of the SPCZ (Widlansky et al., 2011).
- To assess the contribution of synoptic and intraseasonal variability to extreme events, a band-pass Lanczos filter is used to split 200 hPa geopotential height in two frequency bands: synoptic (3-10 days) and intraseasonal (20-90 days).

Results SACZ (A)

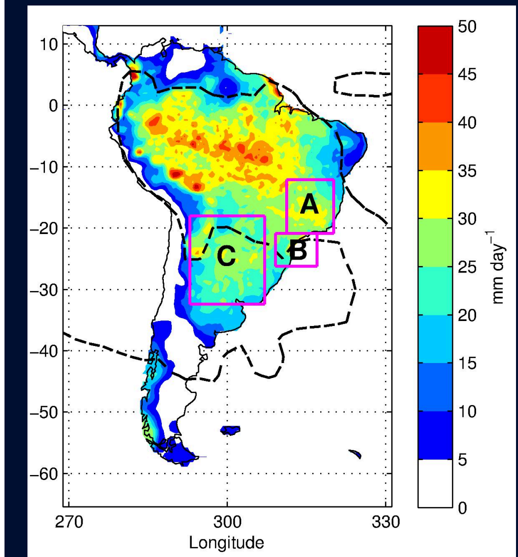

Results SACZ

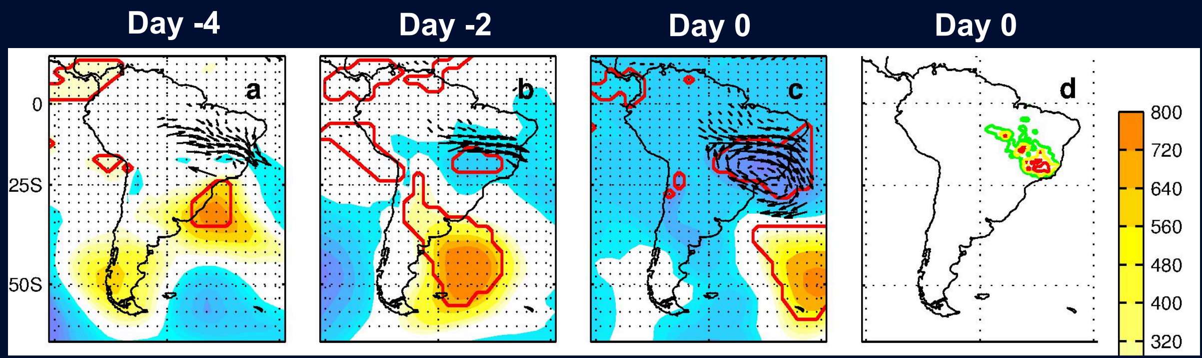

Composites of synoptic evolution of extreme rainfall events in the SACZ for days -4 (a), -2 (b) and day 0 (c), during neutral ENSO summers . Shading represents SLP anomalies, arrows represent 850 hPa anomalous wind vectors (only vectors significant at 95% are plotted), and red contours represent SLP significance (95%). Figure (d) displays the area-averaged 95th percentile rainfall rate (green), the 95th percentile + 5 mm day^{-1} (yellow), and the 95th percentile + 10 mm day^{-1} (red) on composite day 0.

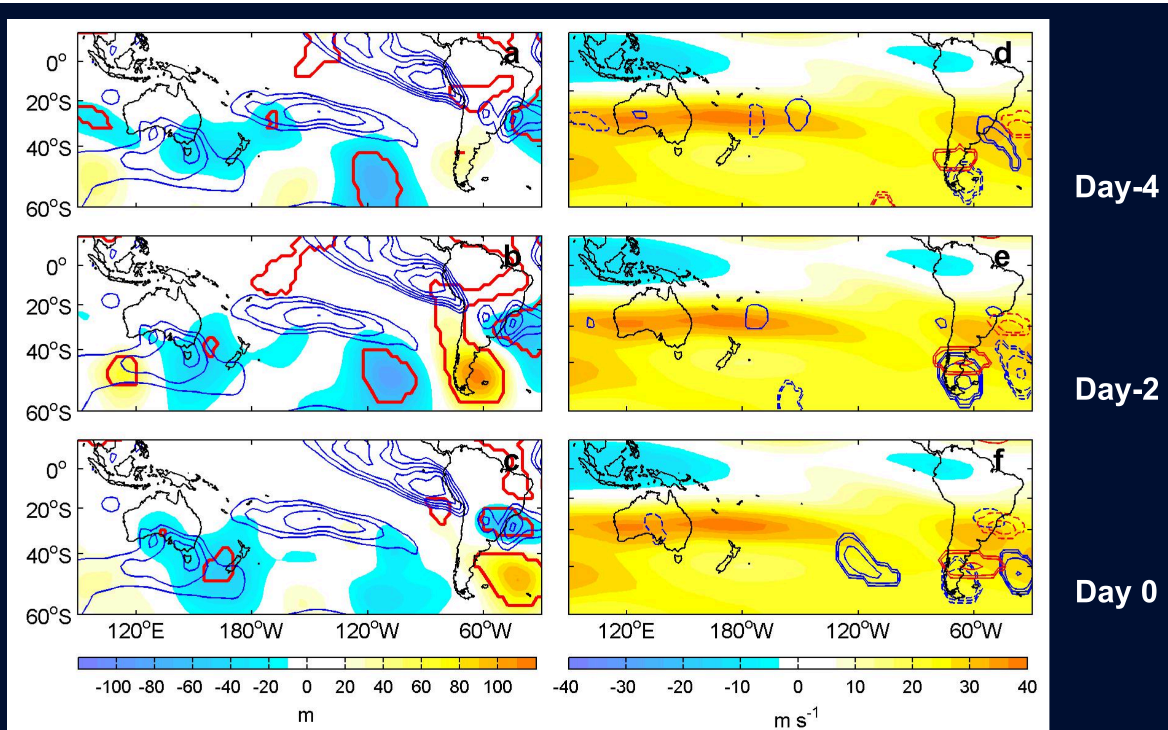

Panels a-c: shading are 200 hPa geopotential height anomalies, with red contours indicating significant anomalies at 95%. Blue contours is 200 hPa negative zonal stretching deformation ($\partial\bar{U}/\partial x < 0$). Negative zonal stretching deformation increases the longitudinal wavenumber, leading to a reduction of the longitudinal wave speed and increasing wave energy density (wave accumulation). This results in intense convective activity. Panels d-f: shading represents 200 hPa $\bar{U}$, and the contours represent filtered 3-10-(blue) and 20-90-day (red) 200 hPa geopotential height anomalies at 10 m intervals.

MJO influence on SACZ extremes

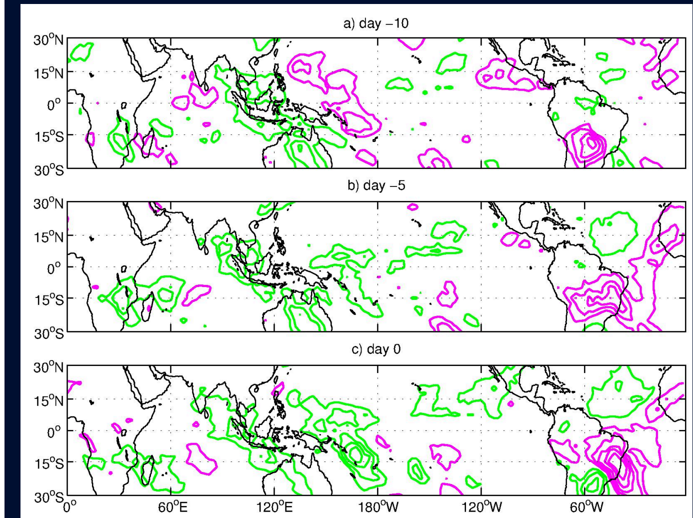

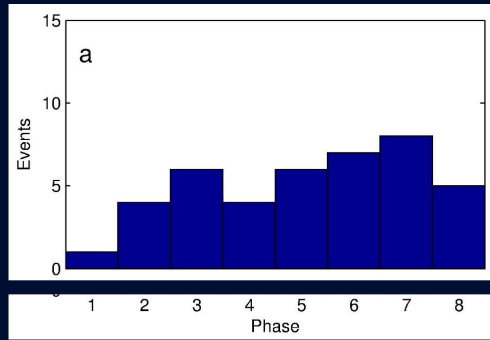

(Left) Composite cycle of intraseasonal OLR anomalies, from day -10 to day 0 for SACZ extreme events during neutral ENSO phases. Magenta (green) lines represent negative (positive) anomalies. Contour interval is 2.5 Wm^{-2}. These anomalies are reminiscent of phases 7, 8 and 1 of MJO.

(Right) 39% of all SACZ extreme events are preceded, 10 days before, by MJO convection on phases 6 and 7, especially phase 7.

Intraseasonal variability

Intraseasonal Variability in South America

(10-100 day band)

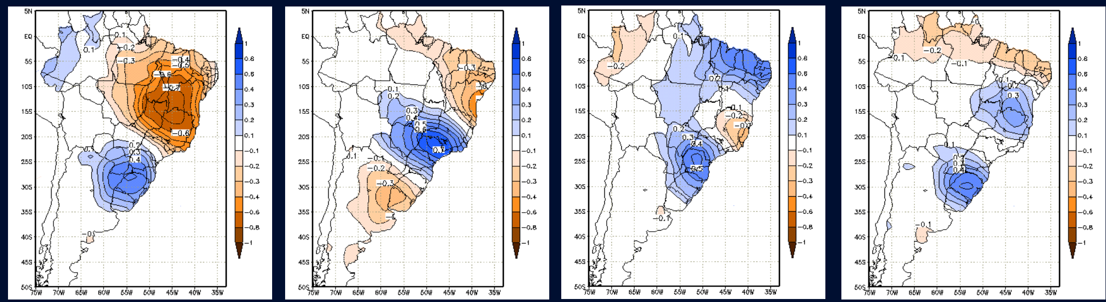

First four EOFs of precipitation, explaining 37,3 % of the intraseasonal variance

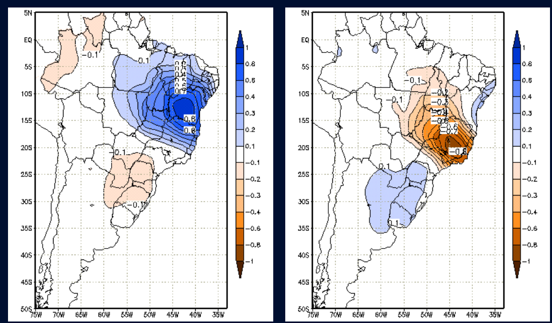

First two rotated EOFs, explaining 17.2 % of the intraseasonal variance.

(Ferraz 2004)

Intraseasonal Variability in South America (30-70 day band)

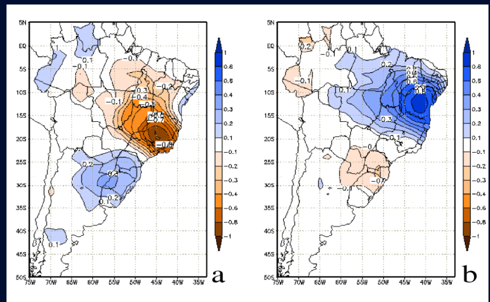

REOF1 REOF2

(Left) First two rotated modes of intraseasonal variability in the 30-70 day band (10.6% and 10.3% of the variance). (Right) Composites of rainfall anomalies and vertically integrated moisture flux for wet and dry phases of these modes. Only significant anomalies are represented by arrows.

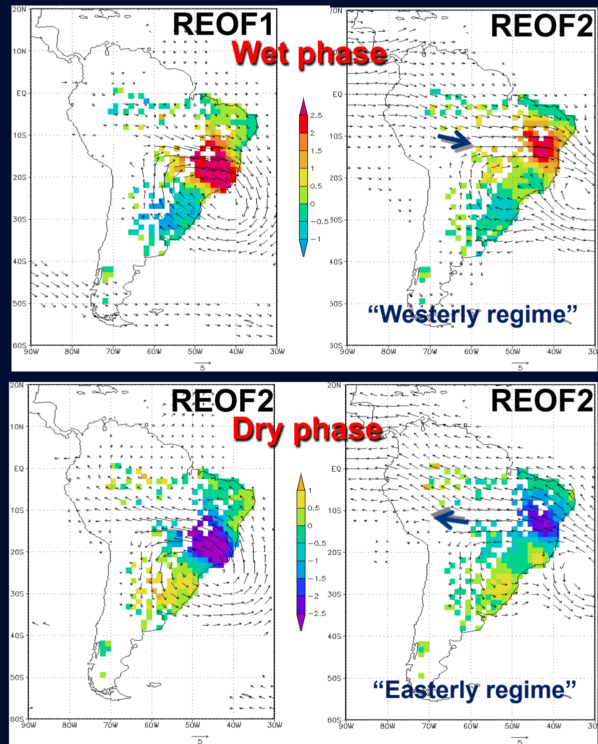

REOF1 REOF2

Ferraz 2004; Grimm and Ambrizzi 2009

MJO impact on South America

Observations

(and simple model simulations)

(Grimm, 2016, in preparation)

Methods

★ Data used: observed daily precipitation from more than 10,000 stations, gridded to 1º, and NCEP/NCAR Reanalysis, in the period 1979-2009. The data are submitted to a bandpass Lanczos filter, which retains intraseasonal oscillations in the 20-90 day band.

★ The impacts of the Madden-Julian Oscillation over South America are assessed for each of the eight phases of the MJO defined by Wheeler and Hendon (2004), according to the following steps:

★ - Multivariate EOF analysis of 15ºS to 15ºN averaged OLR, u850 and u200, after removal of the annual cycle and interannual variability and normalization by the standard deviation;

★ - first two combined EOFs describe propagating MJO structure;

★ - the indices RMM1 and RMM2 (RMM = Realtime Multivariate MJO index) are determined by projecting OLR, u850, and u200 onto the first 2 combined EOFs.

★ - phases are defined according to the combination of these indices.

★ Composites of precipitation anomalies, differences in the frequency of extreme events, and atmospheric fields are made for each phase, and their significance is assessed with a non-parametric test.

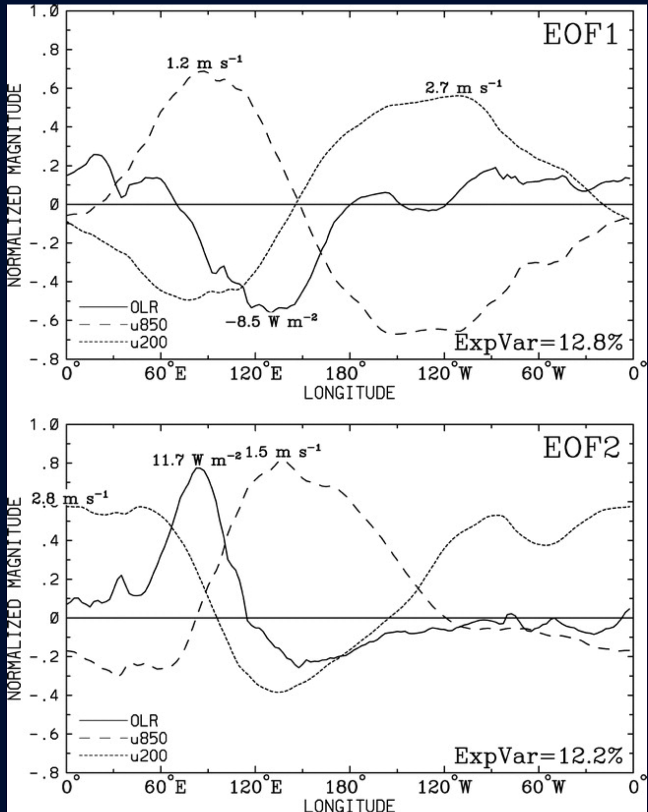

FIG. 1. Spatial structures of EOFs 1 and 2 of the combined analysis of OLR, u850, and u200.

(From Wheeler and Hendon, 2004)

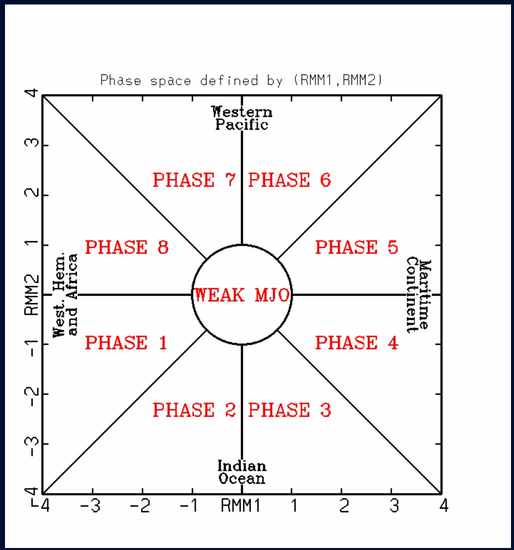

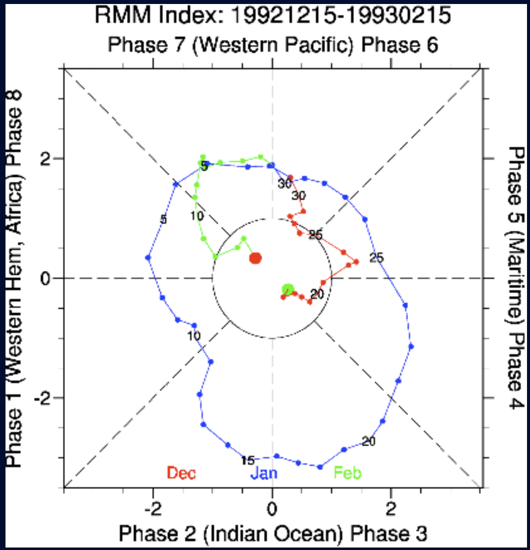

The resulting pair of PC time series that form the desired index is called the Real-time Multivariate MJO series 1 (RMM1) and 2 (RMM2).

(From Wheeler and Hendon, 2004)

SH Summer MJO Div_{200hPa} anomalies

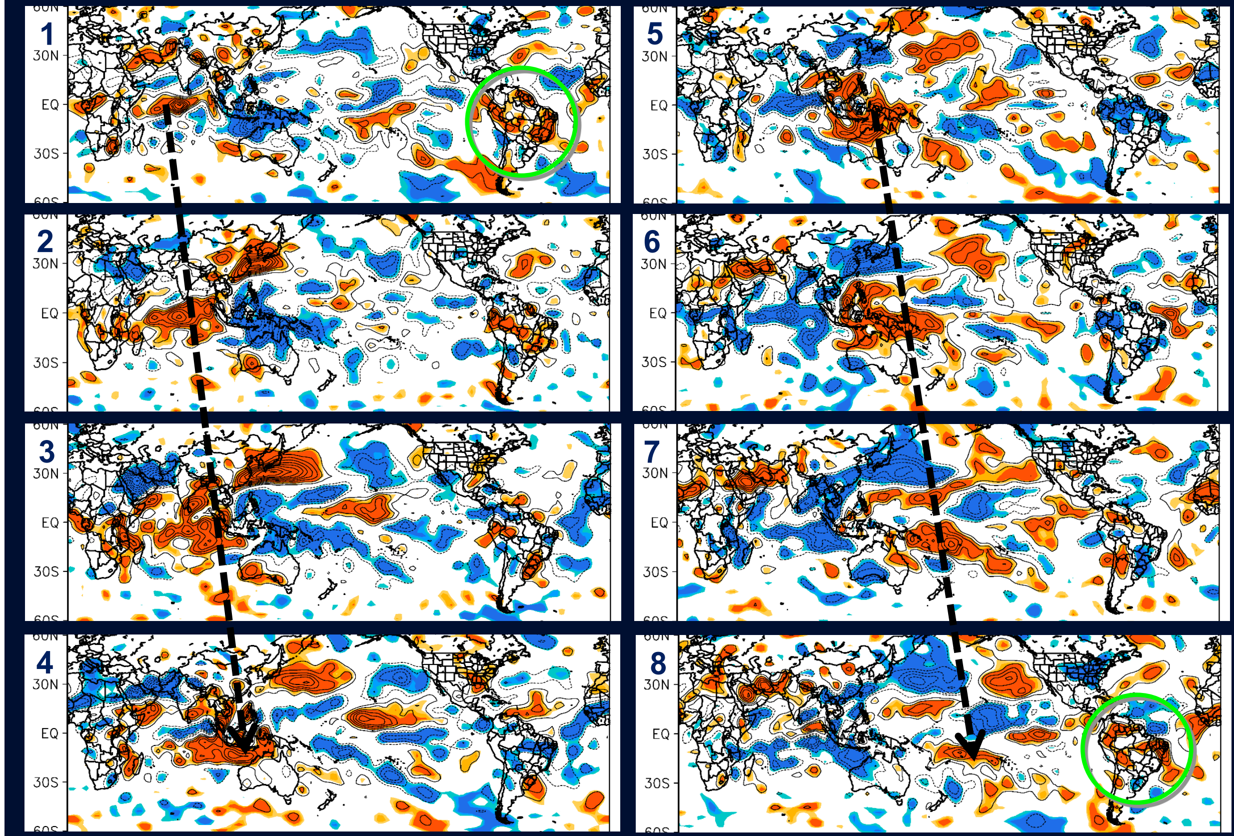

South America summer
MJO-related daily precipitation anomalies

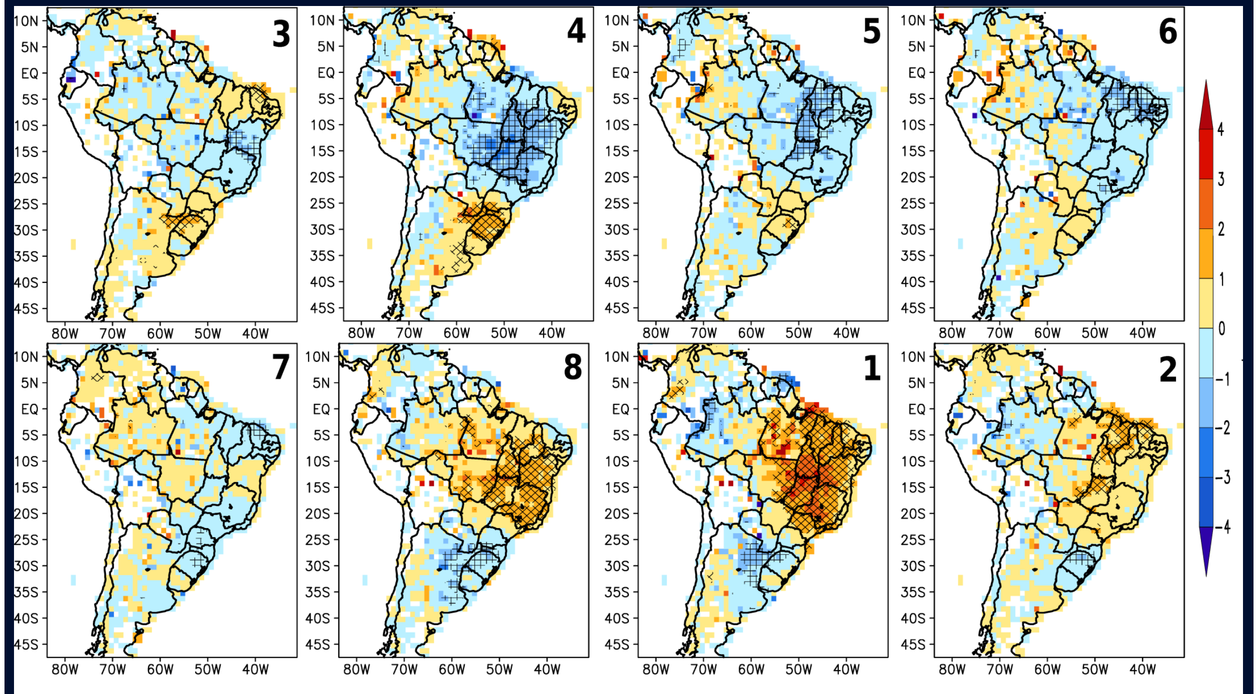

In central-east South America there is up to 4 mm more daily precipitation on average during phase 1 of MJO.

South America summer MJO-related anomalies in frequency of extreme events

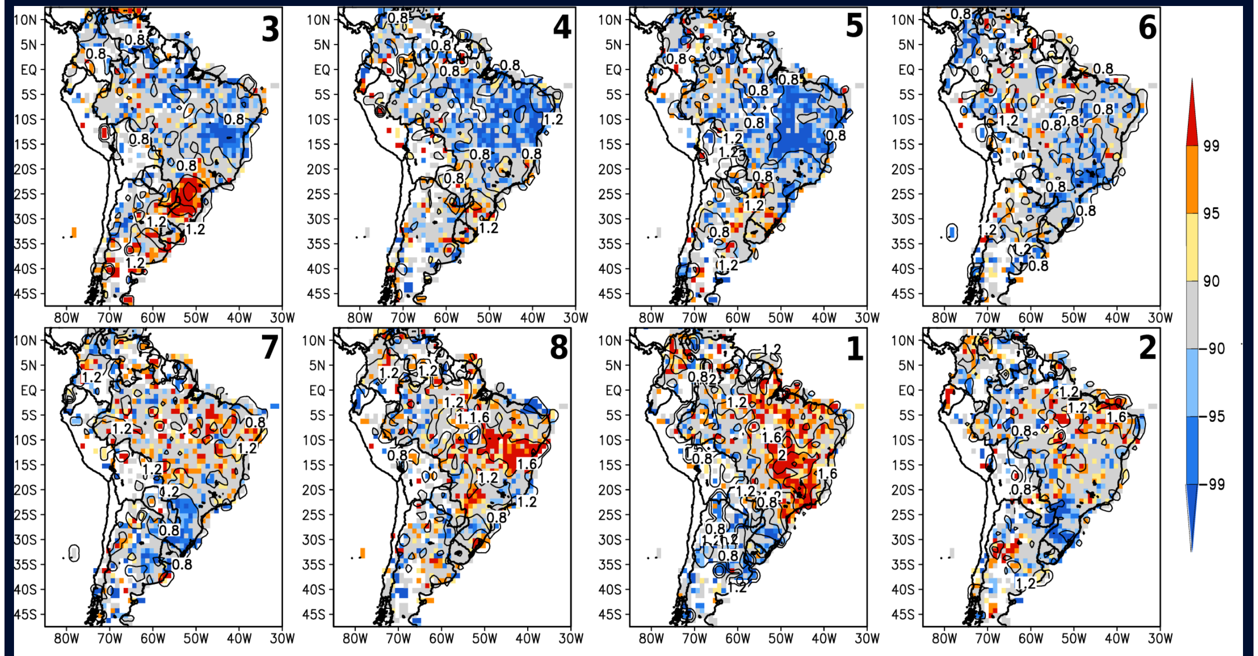

In central-east South America there are twice more extreme rainfall events in MJO phase 1. In southeast South America, they increase by a factor 1.6 in phase 3.

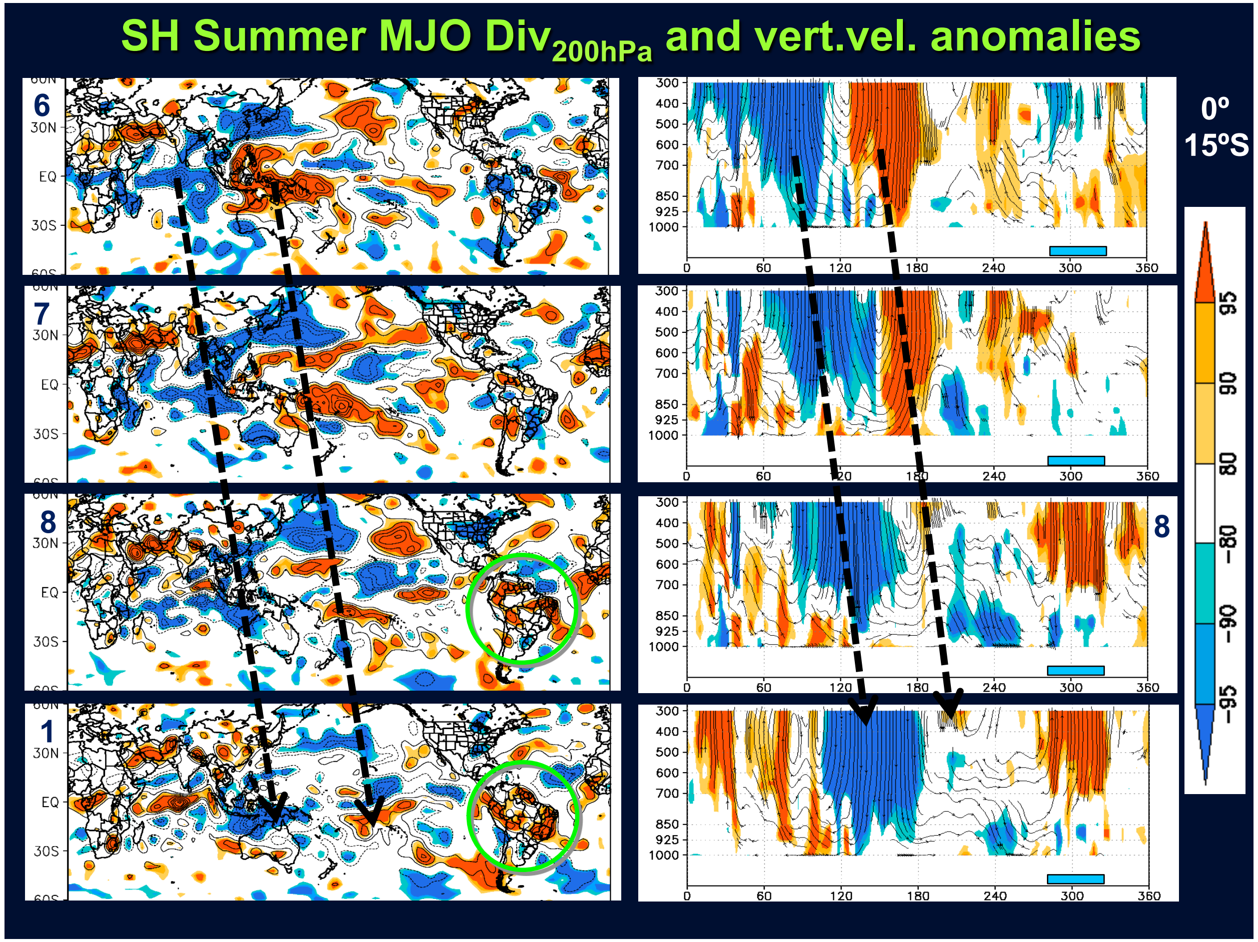

SH Summer MJO Div$_{200hPa}$ and vert.vel. anomalies
6
7
8
1
0º
15ºS
95
90
80
-80
-90
-95

Anomalies Div_{200hPa} e Ψ_{200hPa} – MJO – SH Summer

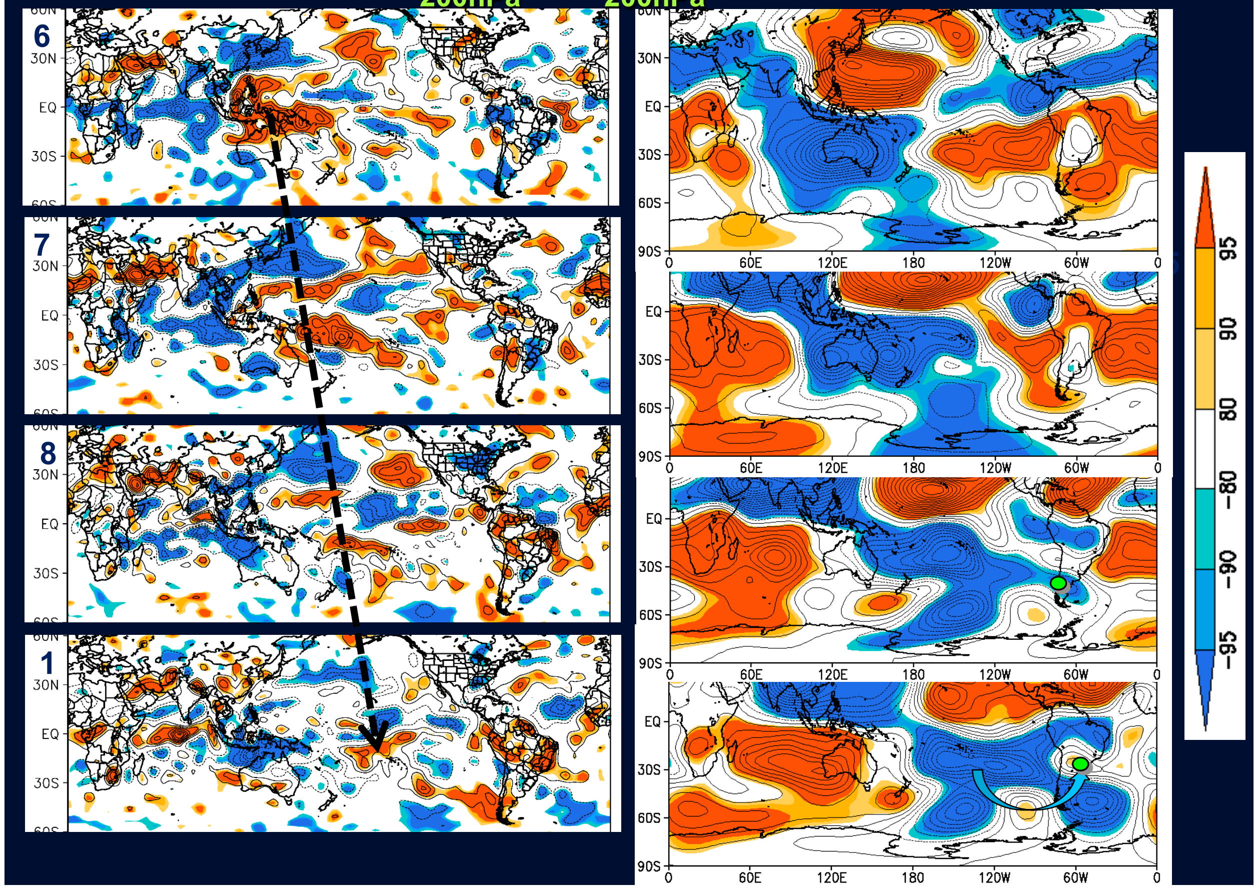

Teleconnection to South America in summer

SPCZ - SACZ (Grimm and Silva Dias, 1995, JAS)

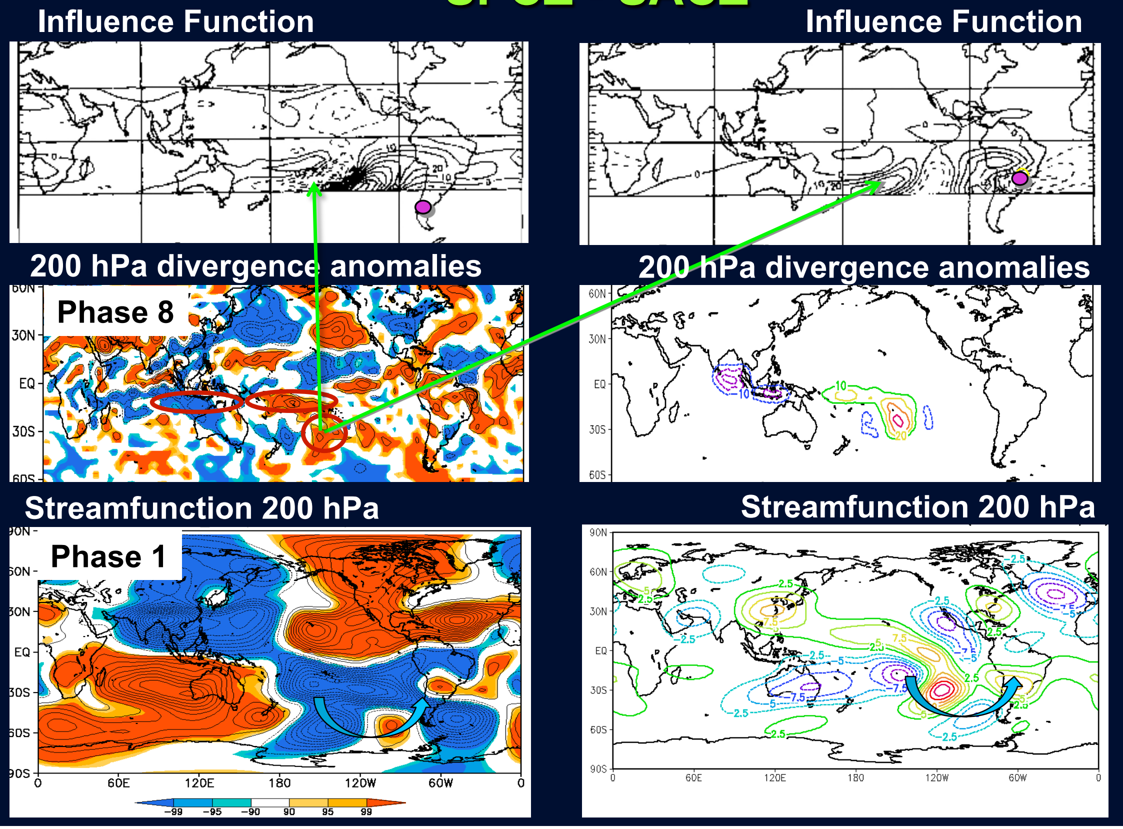

Teleconnection to South America in summer
SPCZ - SACZ

200 hPa divergence anomalies

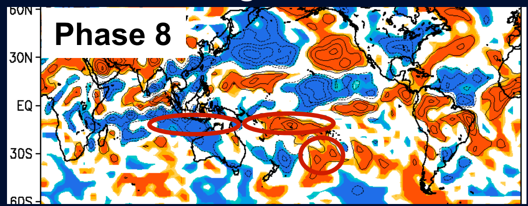

Streamfunction 200 hPa

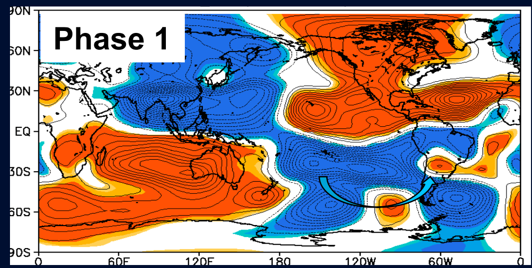

200 hPa divergence anomalies

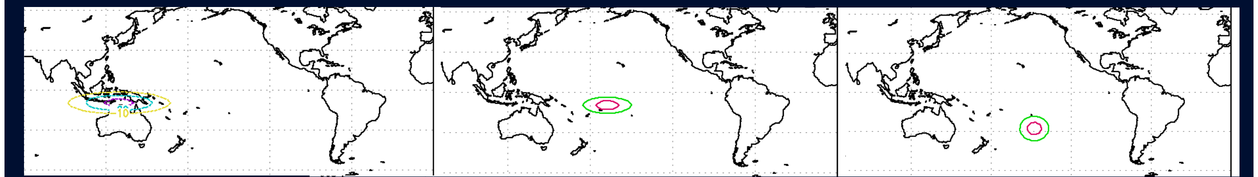

Streamfunction 200 hPa

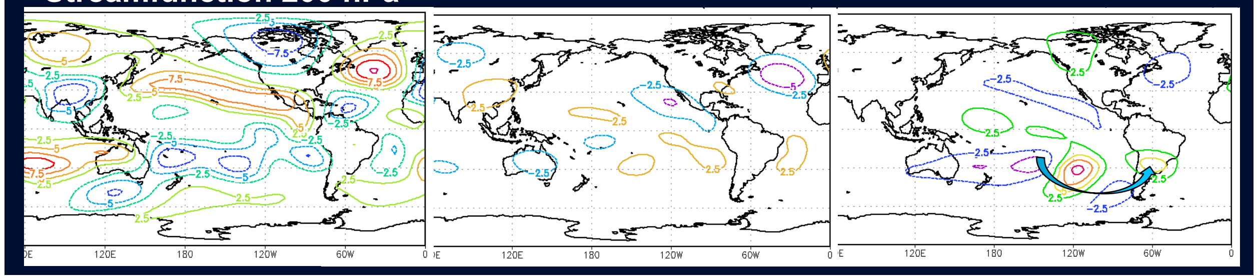

MJO impact on South America

Model CFS v2
Reforecasts 1999-2010

MJO - Model CFS v2

Indices of skill in predicting the MJO phase

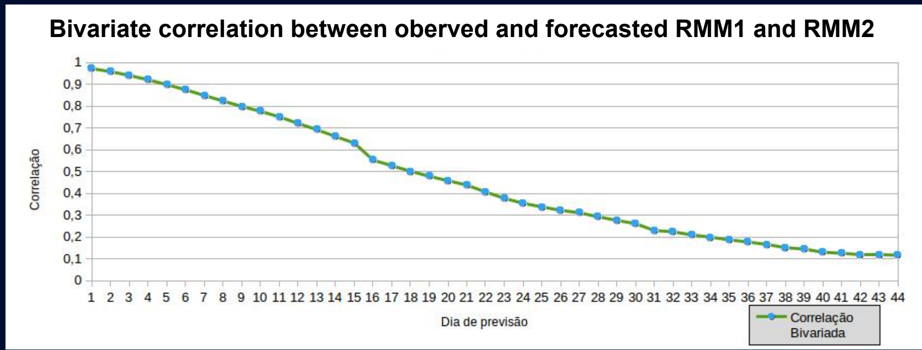

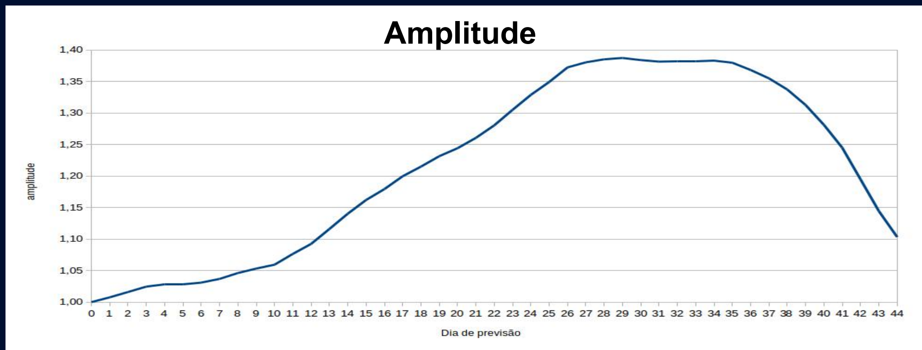

MJO - Model CFS v2

Indices of skill in predicting the MJO phase

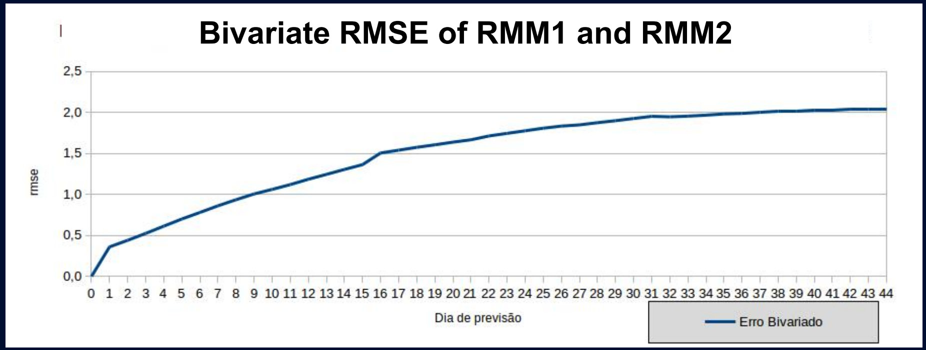

MJO - Model CFS v2

Model Reanalysis- precip. anom. | **Model prediction15-24 day - precip. anom.**

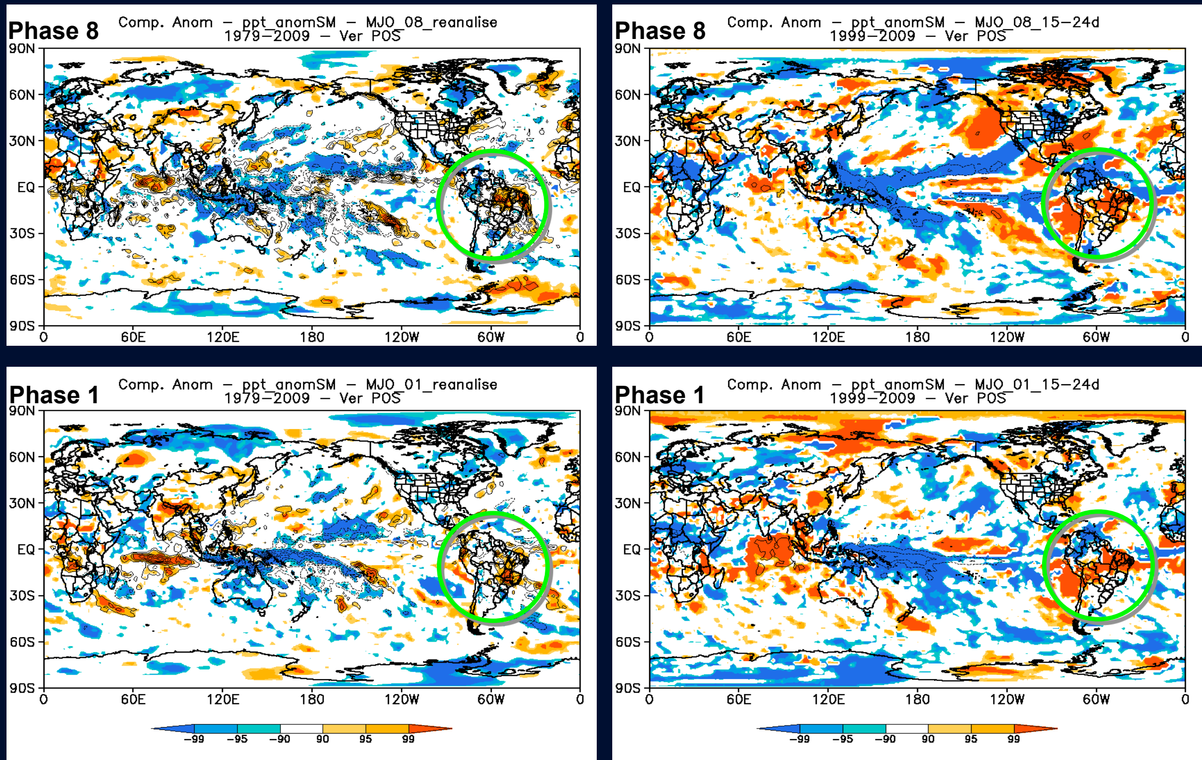

MJO - Model CFS v2

Model Reanalysis | **Model prediction15-24 day**

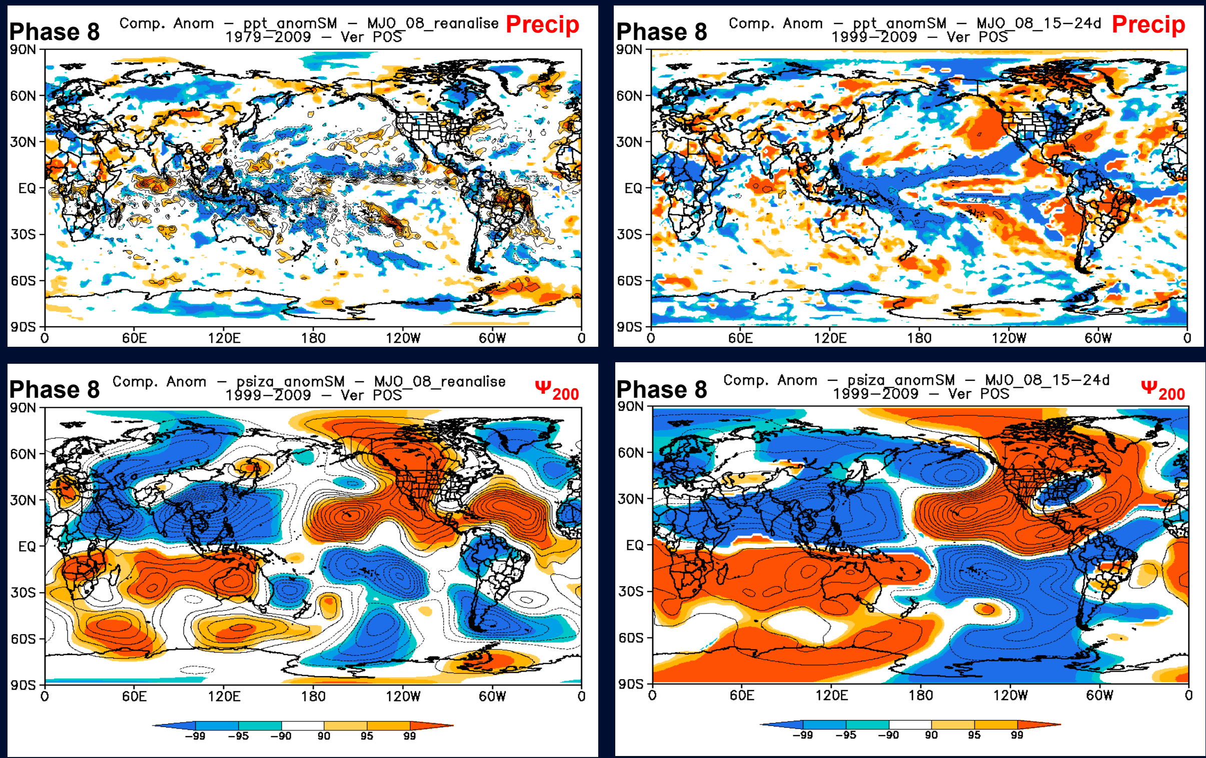

MJO - Model CFS v2

Model Reanalysis | **Model prediction15-24 day**

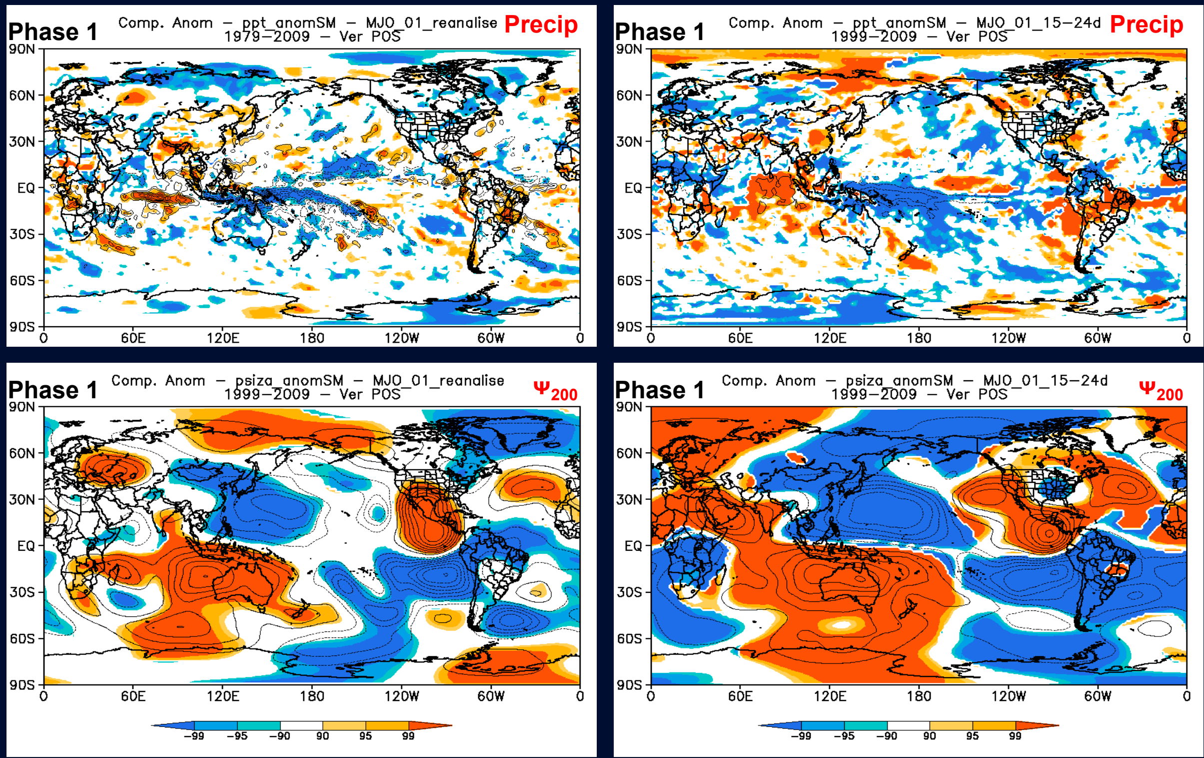

MJO - Model CFS v2

Model prediction 15-24 day | **Model prediction 25-34 day**

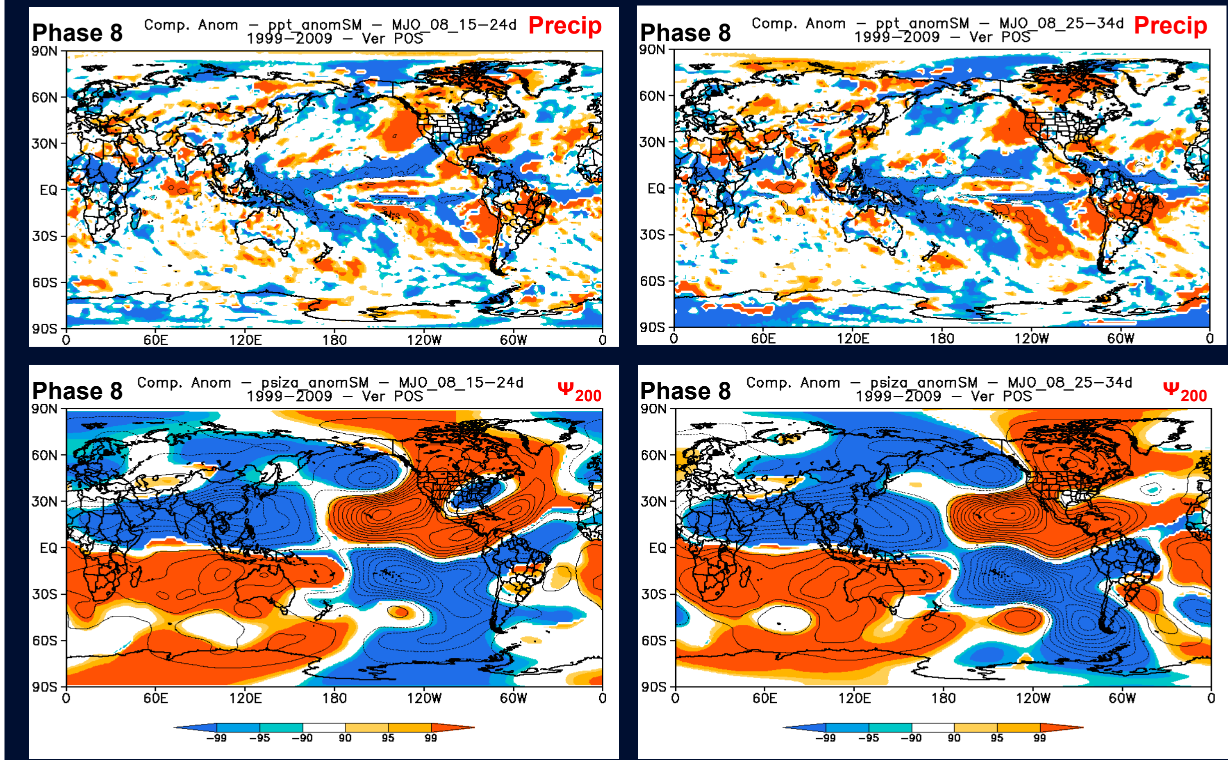

MJO - Model CFS v2

Model prediction 15-24 day | Model prediction 25-34 day

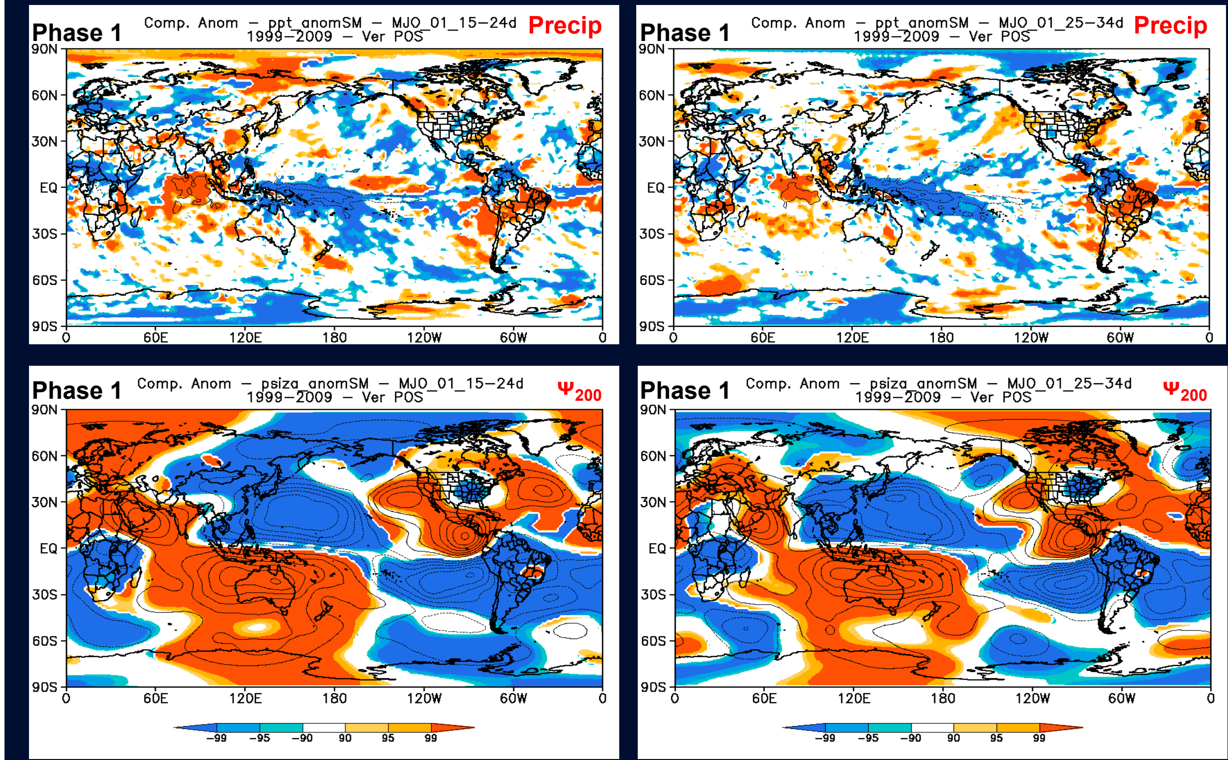

Madden-Julian Oscillation (MJO) GFDL CM4

Nov-Apr life cycle composite using US CLIVAR standard diagnostic package

OBS (AVHRR)

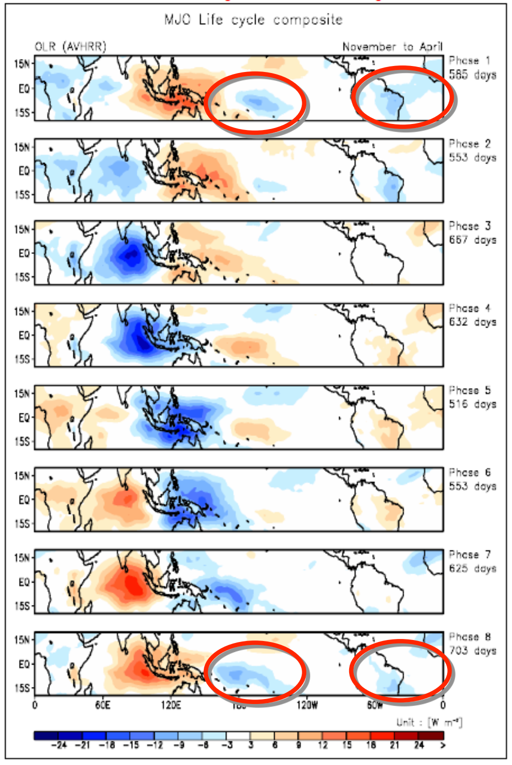

Model

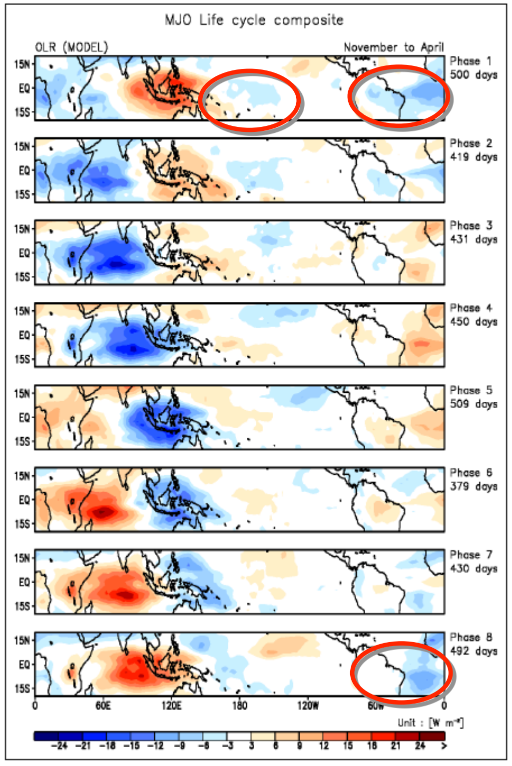

Teleconnections with southern Africa

Data and Methods

- Observed daily precipitation data from both continents in the period 1979-1999 are gridded to 1°, and in each grid point only intraseasonal oscillations are retained, through a bandpass Lanczos filter.
- NCEP/NCAR Reanalysis data provides atmospheric fields.
- Some regions with different precipitation regimes are selected in South Africa.
- For each season, the filtered precipitation averaged over each of these regions is correlated with filtered precipitation in each 1° x 1° grid box with data over South America. In such correlation, lags from 0 up to 5 days are applied to the African data, in order to disclose convection anomalies over South America that could produce atmospheric perturbations associated with the precipitation anomalies over South Africa.
- The 200 hPa streamfunction anomalies associated with daily precipitation above 1 standard deviation in the filtered series of the African regions under focus are composited for each season.
- The influence function analysis for target points in the center of these anomalies indicates that perturbations of the upper level divergence associated with anomalous convection over South America are able to produce the atmospheric circulation anomalies associated with enhanced precipitation in those regions of South Africa.

Precipitation regimes

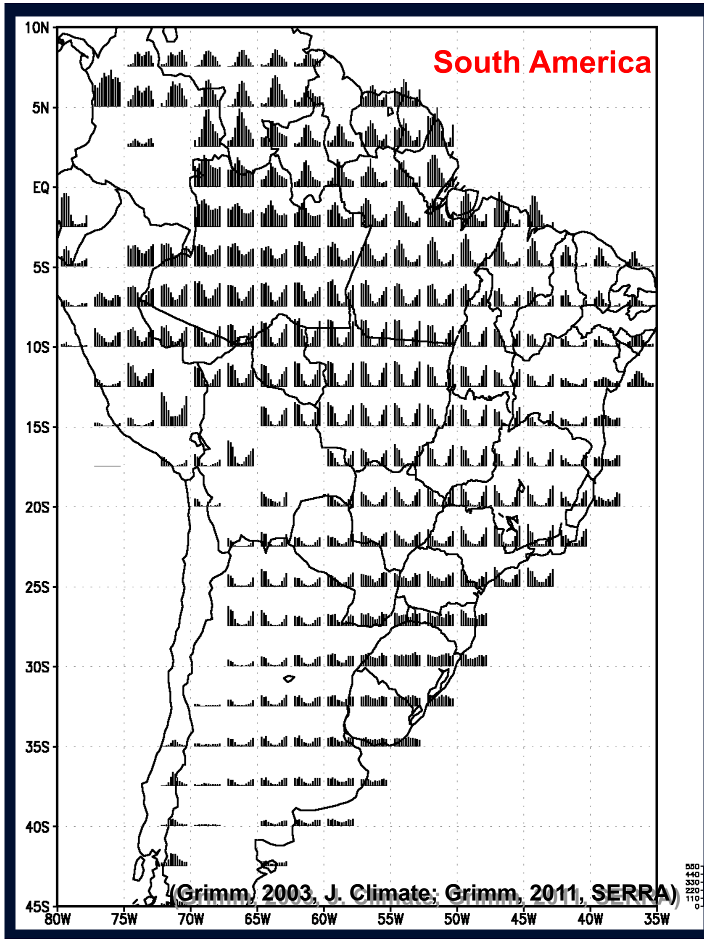

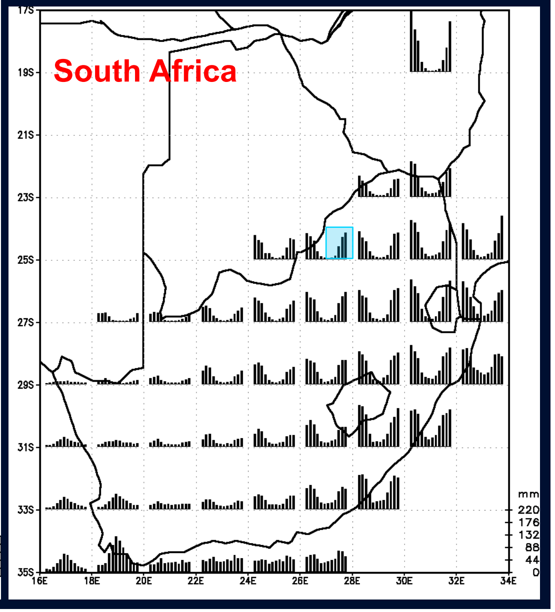

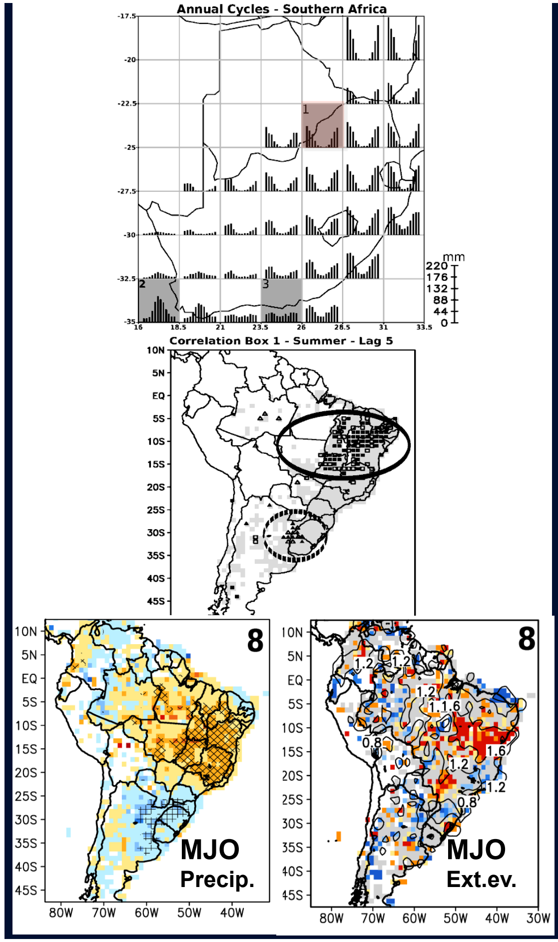

Significant correlation between South America and South Africa rainfall

Grimm, A. M. and C. J. C. Reason, 2015: Intraseasonal teleconnections between South America and South Africa. *Journal of Climate*.

(Upper panel) Selected regions and annual cycles of precipitation in South Africa. (Central panel) 1 degree boxes in South America with precipitation significantly correlated to lagged precipitation (5 days) in selected region 1 in South Africa. Dark squares (triangles) indicate confidence level higher than 90% for positive (negative) correlation; open squares (triangles) are for confidence levels between 85% and 90%. Ellipses indicate regions with maximum correlation. White areas are void of data. (Lower panel) MJO related anomalies for Phase 8.

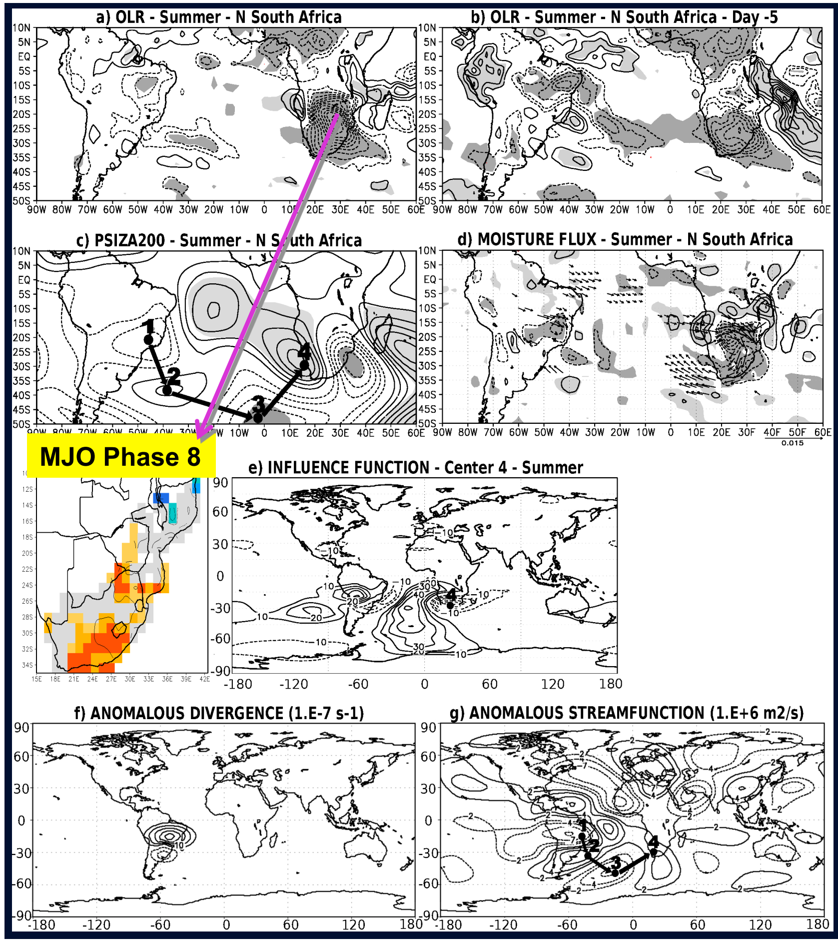

Box1

Austral Summer

Anomaly composites for the days of positive phases in Box 1, in summer: (a) OLR and (b) OLR 5 days before, (c) 200 hPa streamfunction, (d) vertically integrated moisture flux and its divergence. Shades indicate confidence levels higher than 90% for negative (positive) anomalies, and only significant moisture fluxes are shown. (e) Influence function for action center 4. The values shown in each location are proportional to the streamfunction response at the target point to a unitary upper-level divergence anomaly in this location. (f) anomalous 200hPa prescribed divergence and (g) corresponding steady anomalous streamfunction.

Summer teleconnection between SAm and SAf

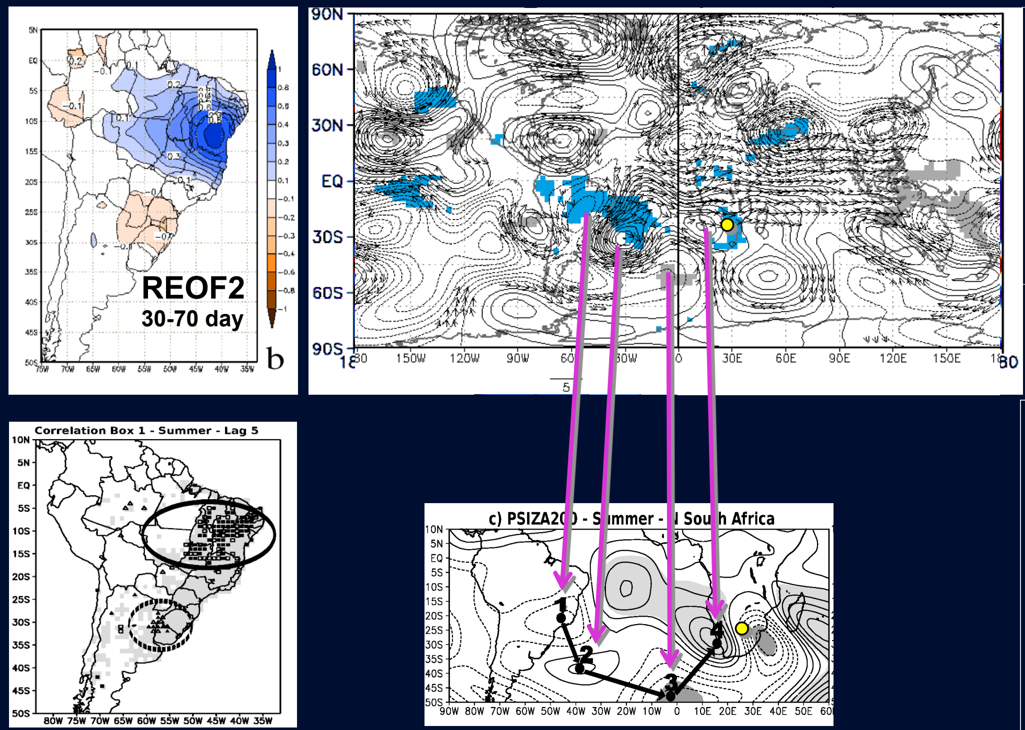

OLR and ψ_{200} anomalies associated with positive phases of the 2nd REOF (> 1.4 σ) in the 30-70 day band

Ψ_{200} anomalies associated with positive phases of the filtered precipitation (20-90 day band) in Box 1 of South Africa

Summer teleconnection between SAm and SAf

Further results

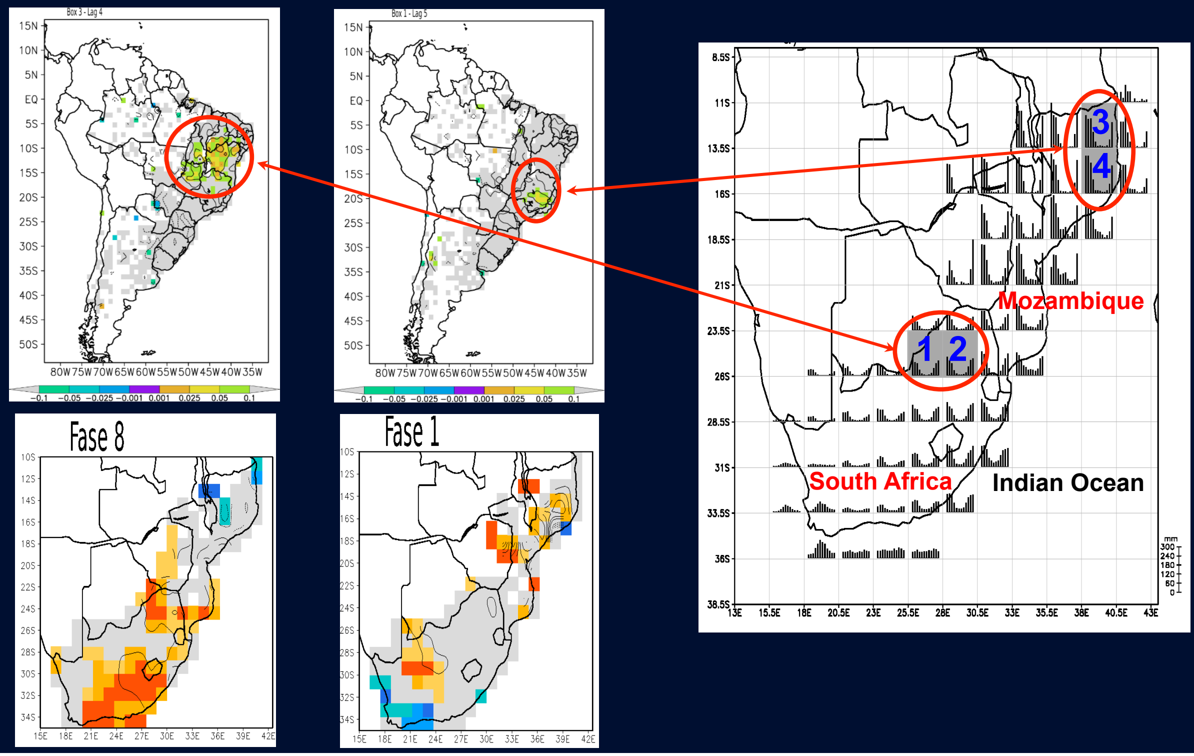

Interannual variability

Relationship between precipitation in Spring and in Summer

Interannual Variability

ENSO-related variations

(Grimm, 2003; 2004)

El Niño | **La Niña** | **El Niño - moisture flux**

Nov

Jan

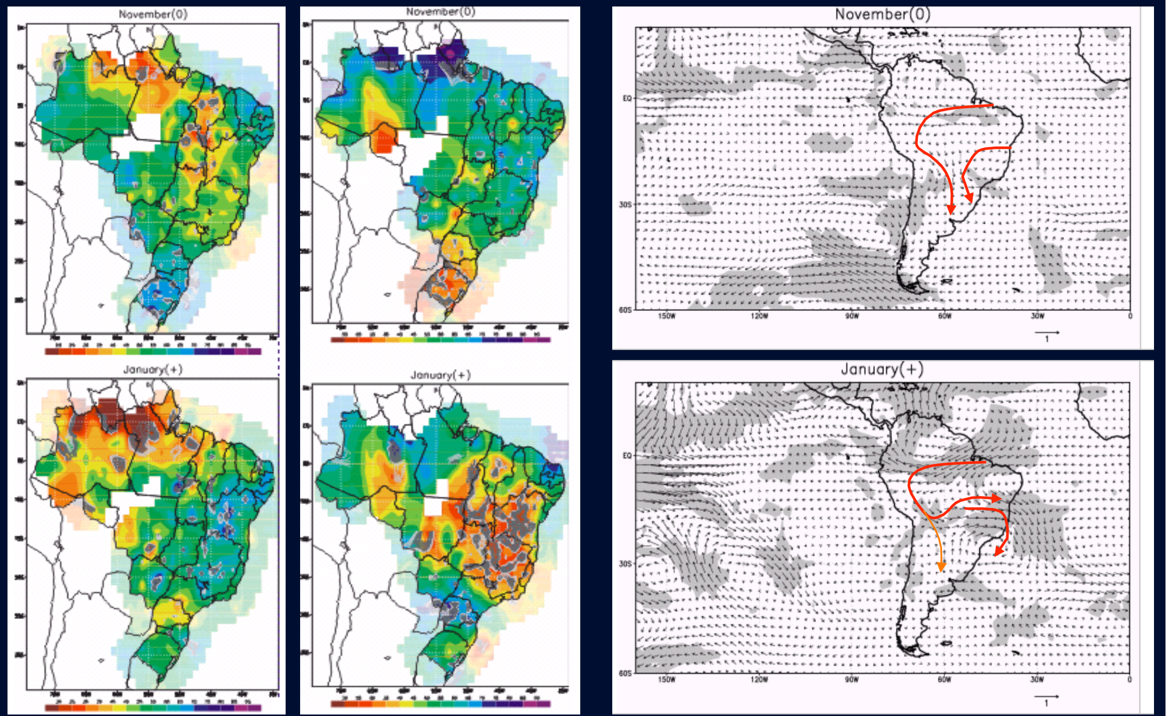

Similar changes from spring to summer happen in other years as well…

SPRING EOFs

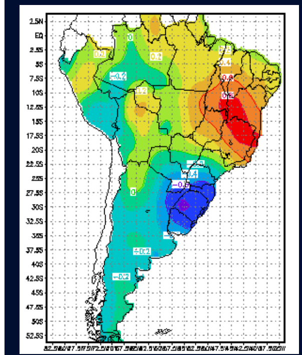

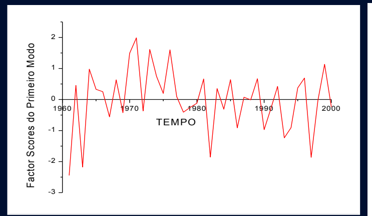

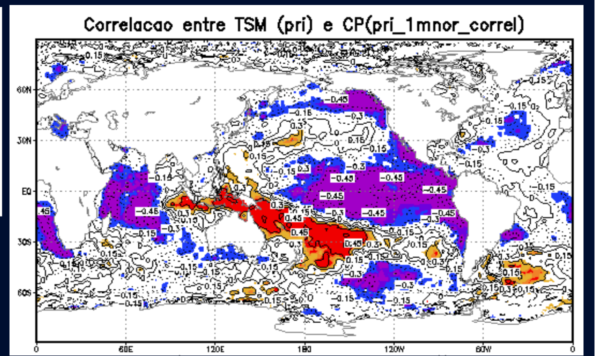

EOF1 - 18.5 %

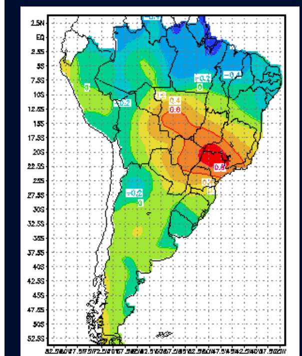

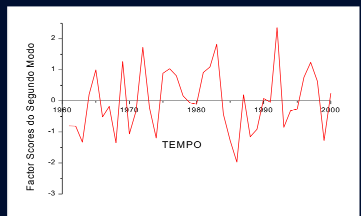

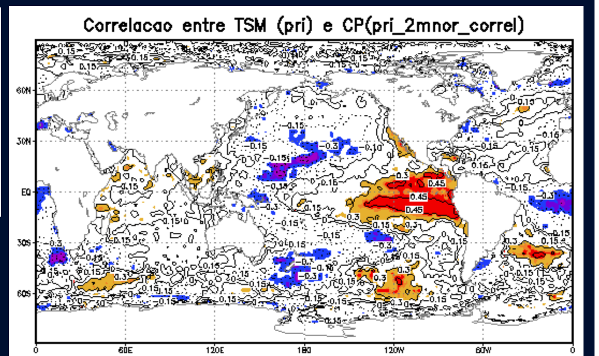

EOF2 - 16.7 %

Grimm and Zilli 2009

SUMMER EOFs

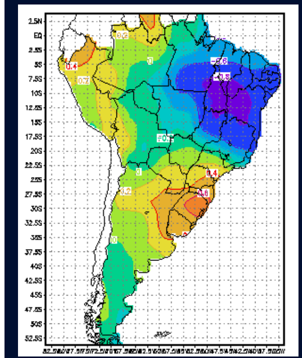

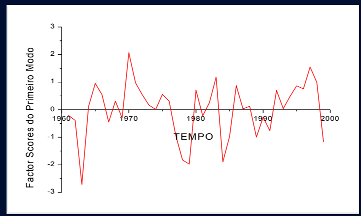

EOF1 - 22.0 %

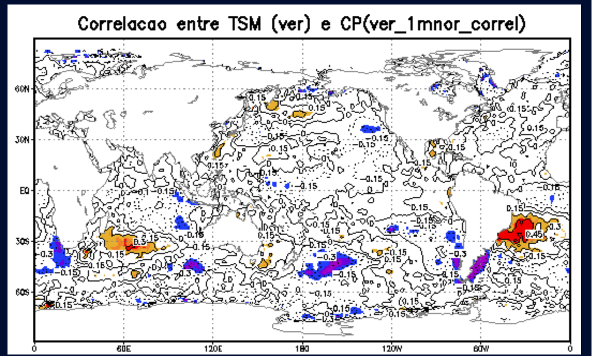

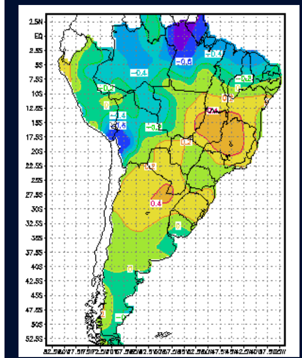

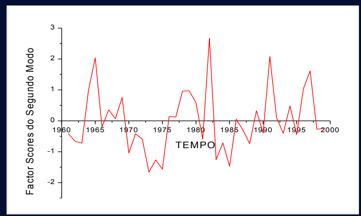

EOF2 - 10.1 %

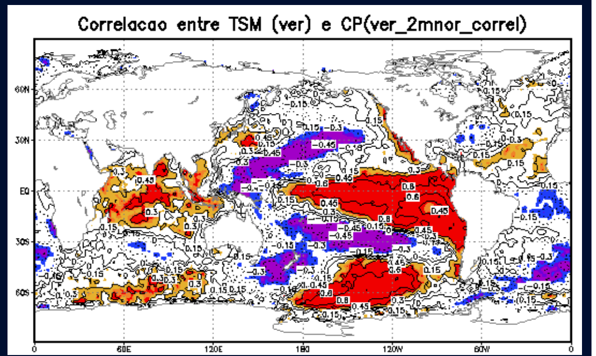

Grimm and Zilli 2009

CORRELATION BETWEEN SPRING AND SUMMER PCs

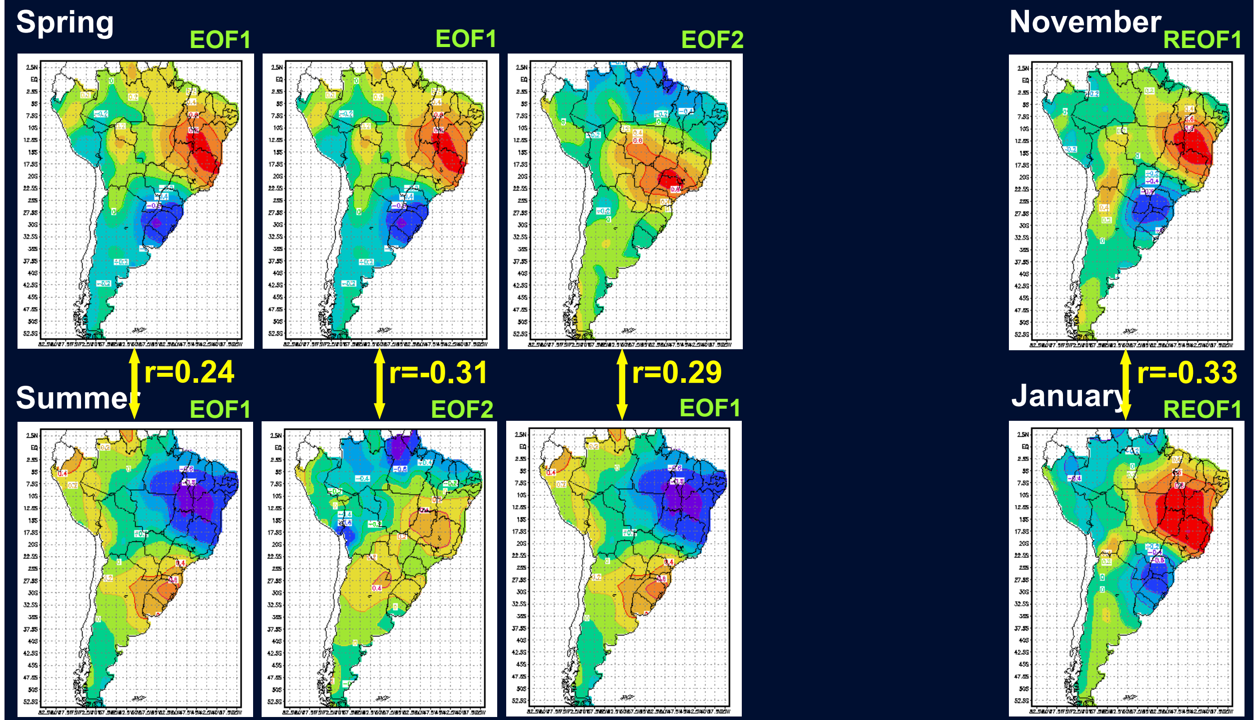

Grimm and Zilli 2009

Evolution of the precipitation in Central-East Brazil

Keyed to Spring and Summer PC1.

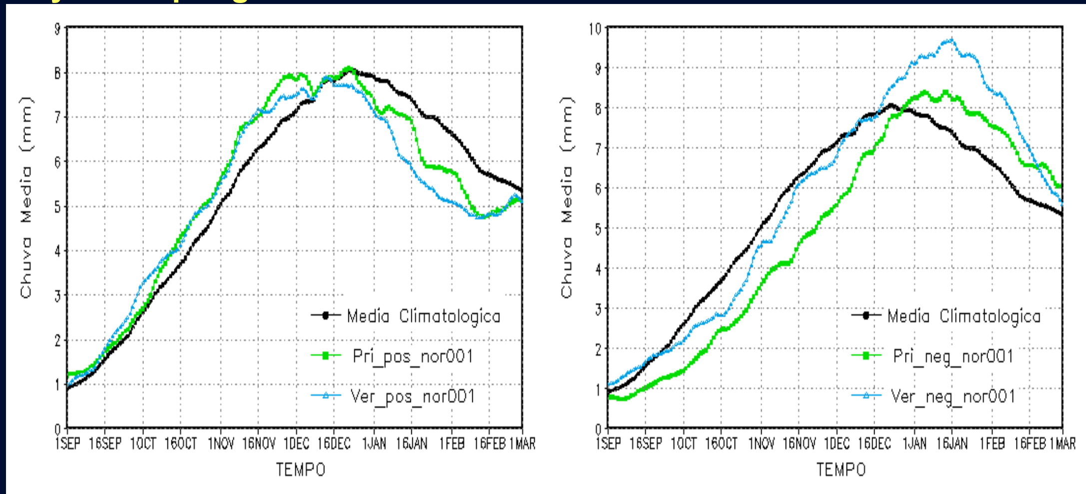

Spring EOF1 **Summer EOF1**

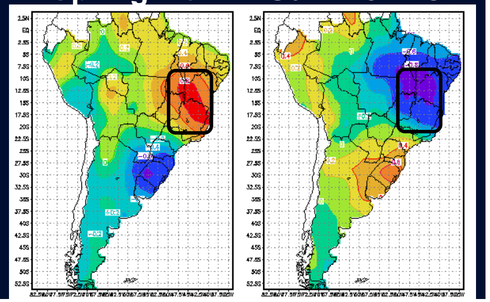

Composite evolution of the 30-day running mean precipitation (mm day-1), averaged over Central-East Brazil for all years (black line) and (left) for years in which spring (summer) PC1 is above 0.5 standard deviation (green (blue) line) or (right) for years in which spring (summer) PC1 is below -0.5 standard deviation (green (blue) line).

(Grimm and Zilli 2009)

MODELING STUDIES

(Grimm, Pal and Giorgi 2007)

Response to reduced soil moisture

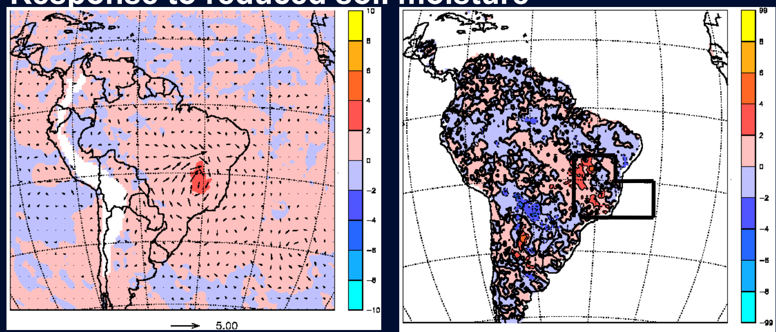

Response to reduced topography in eastern S. America

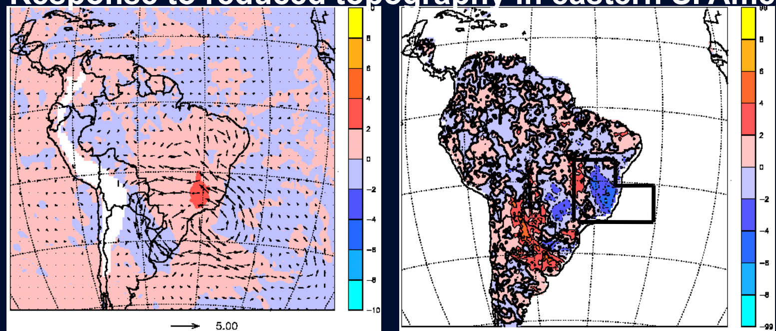

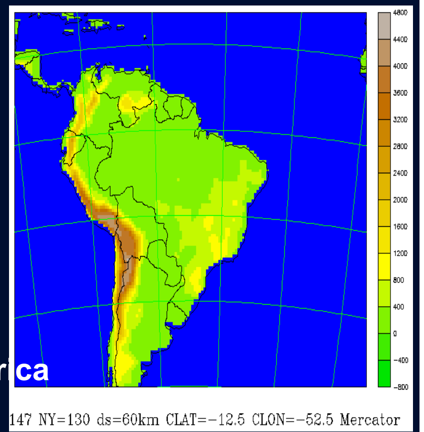

Realistic topography in eastern South America

HYPOTHESIS

(Grimm, Pal and Giorgi 2007)

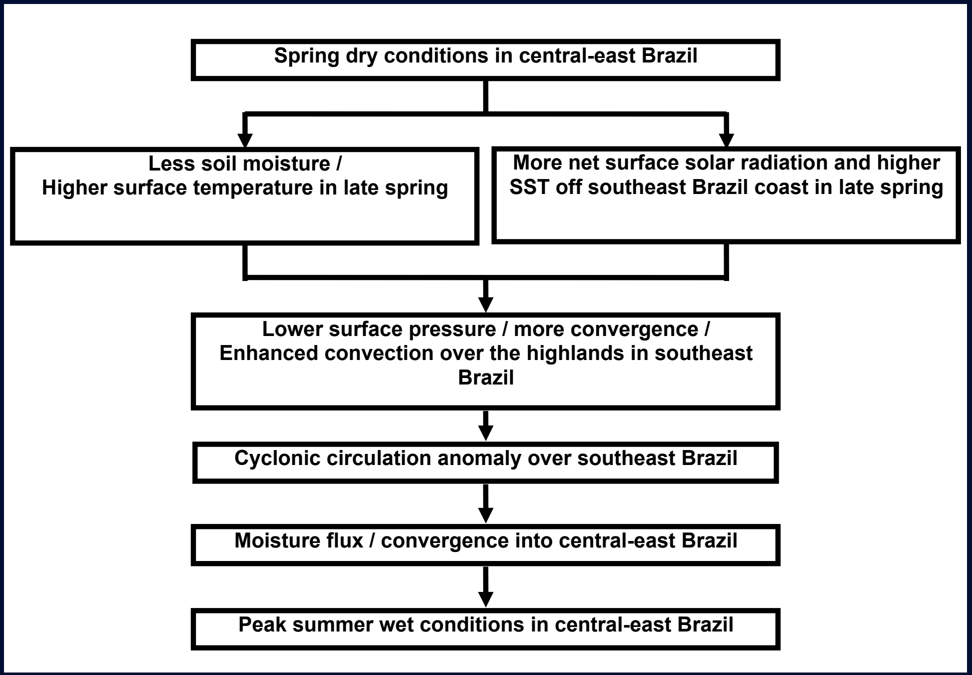

Diagram of the pathway through which spring anomalous dry conditions may lead to subsequent peak summer wet conditions in central-east Brazil. The above diagram is also valid for opposite anomalies, starting from spring wet conditions in central-east Brazil.

SCHEMATIC DIAGRAM OF SPRING-SUMMER INVERSE RELATIONSHIP

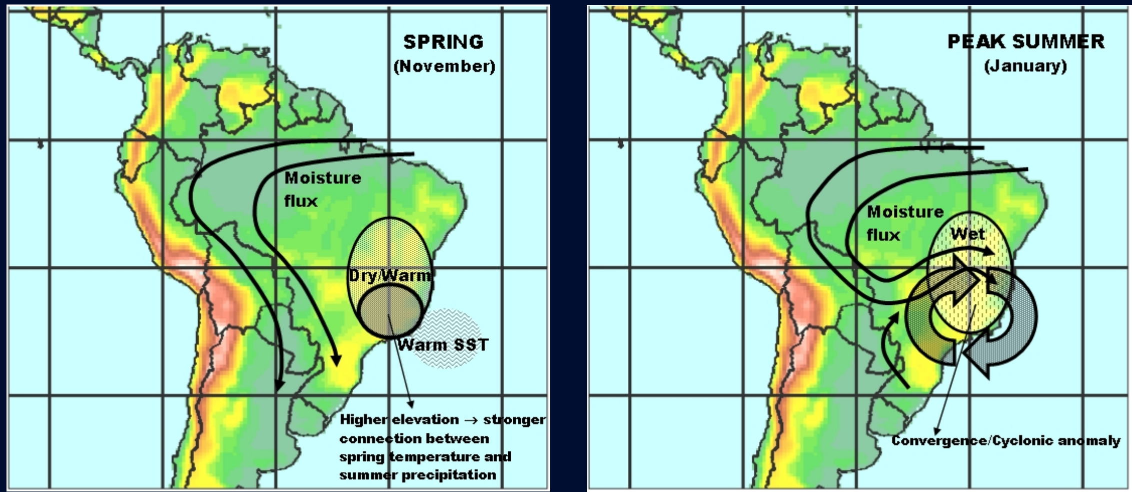

Schematic evolution from (a) spring dry conditions to (b) peak summer wet conditions in Central-east Brazil, through decreasing low-level pressure, convergence and cyclonic anomaly over southeast Brazil.
(Grimm, Pal, and Giorgi 2007)

TEMPERATURE-PRECIPITATION RELATIONSHIPS

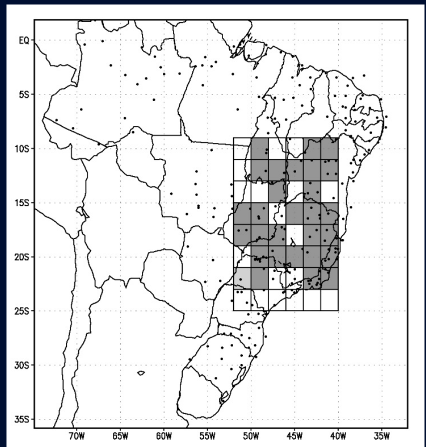

Negative significant correlation of October-November precipitation vs November surface air temperature averaged in 2º X 2º areas (Grimm, Pal and Giorgi 2007).

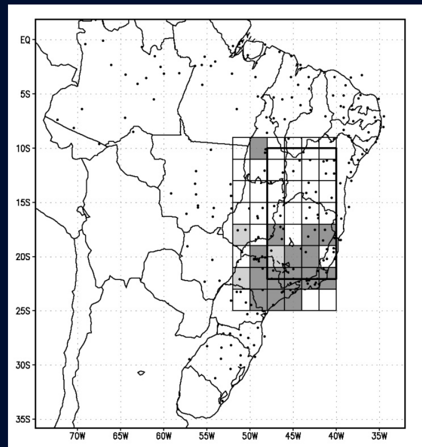

Positive significant correlation of surface air temperature in November vs precipitation averaged in the bold rectangle in January (Grimm, Pal and Giorgi 2007).

TEMPERATURE-PRECIPITATION RELATIONSHIPS

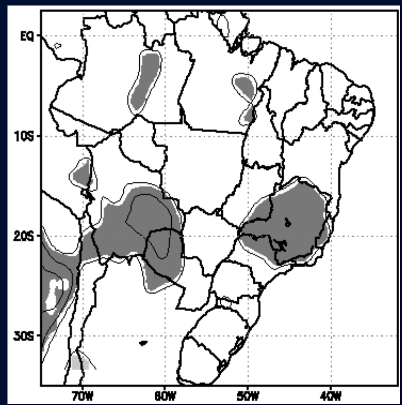

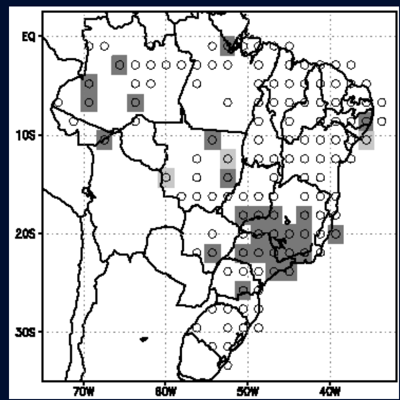

Correlation between PC1 of January precipitation and temperature at 2m in November obtained from (a) NCEP/NCAR Reanalysis data), (b) station data. Positive (negative) correlation coefficients with significance level better than 0.10 are indicated by dark (light) shaded areas; contours start at ±0.2 and the interval is 0.1 (Grimm and Zilli 2009).

Soil Moisture Controls on Evaporation

- Over many parts of the world, there is a range of SM over which evaporation rates in(de)crease as soil moisture in(de)creases (soil moisture is a limiting factor – moisture controlled).
- Above some amount of moisture in the soil, evaporation levels off.
- In that wet range, moisture is plentiful, and is no longer controlling the partitioning of fluxes (it's energy controlled).

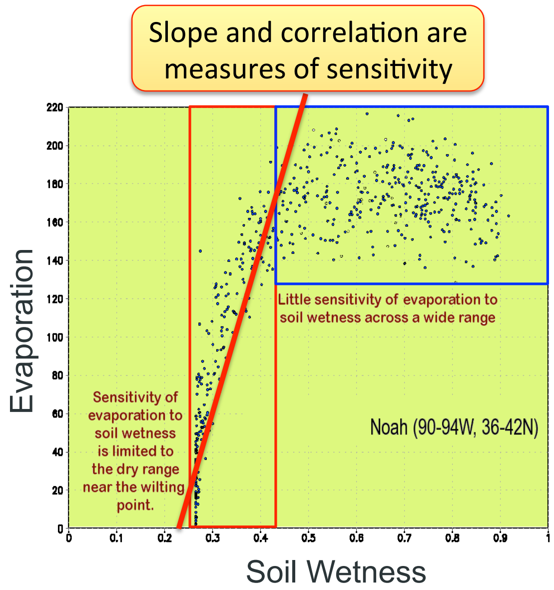

Is this relationship between anomalous rainfall in spring and changes in the temperature (and therefore, in pressure and circulation) coherent with the climatological values of soil moisture in Central-East Brazil?

Climatological percentage of maximum soil water storage

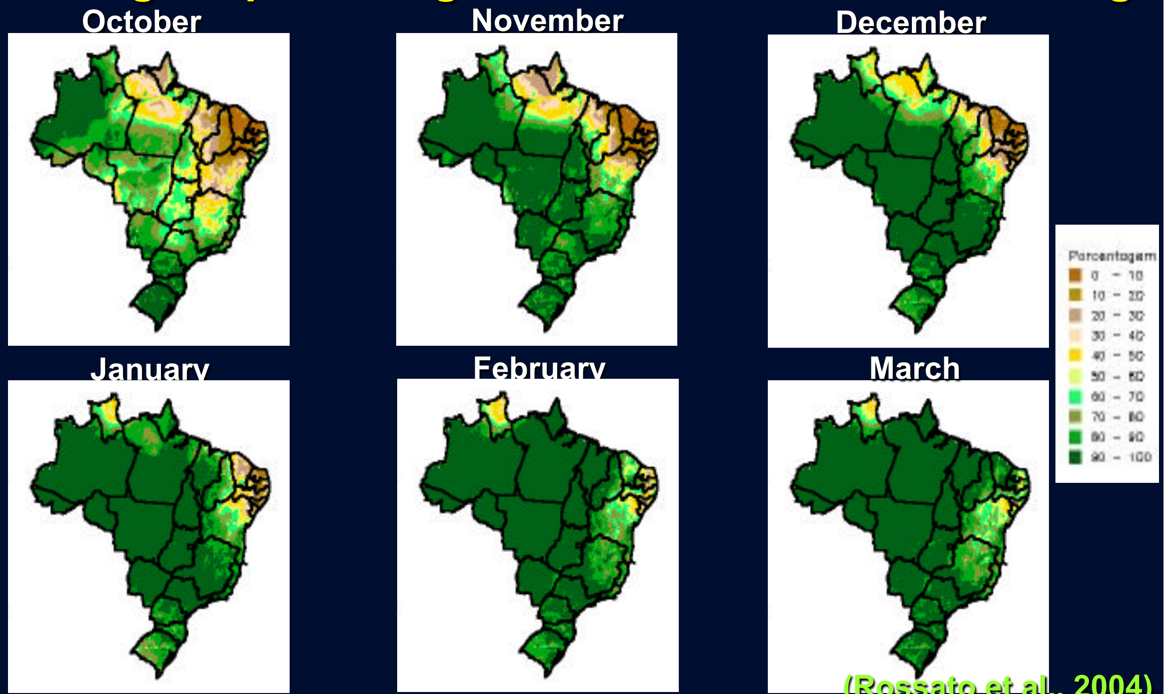

(Rossato et al., 2004)

Verification of the relationship November-January

2001-2007

2000-2001 | 2002-2003 | 2003-2004 | 2005-2006 | 2006-2007

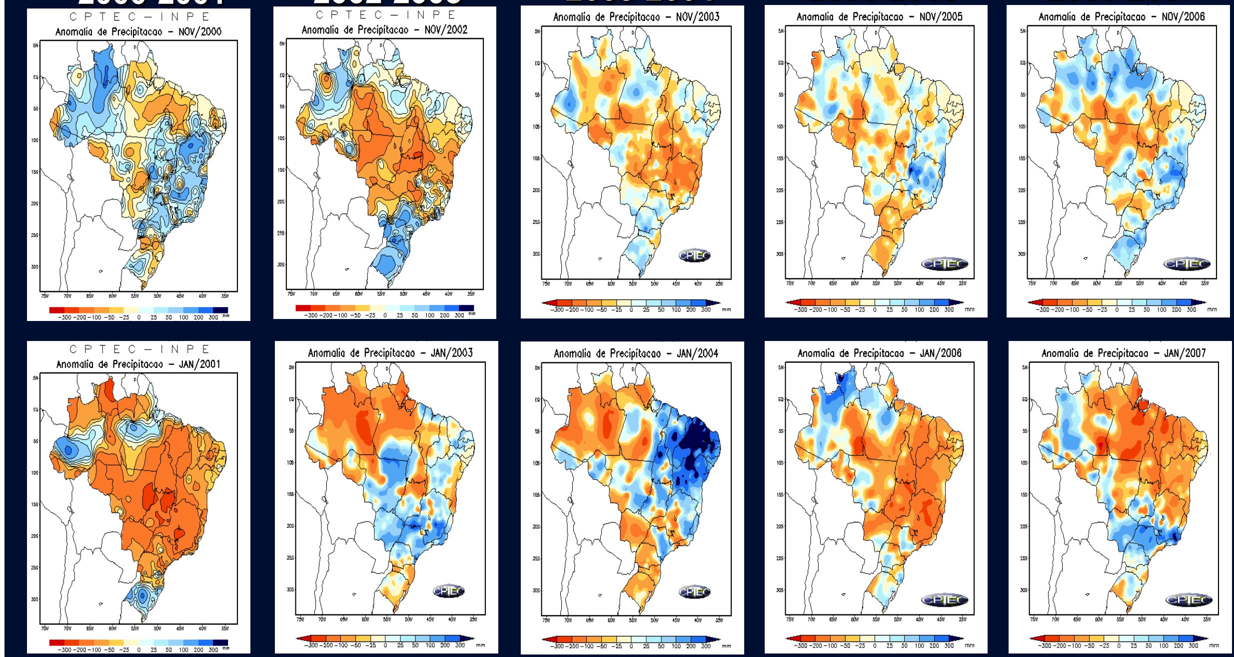

Verification of the relationship November-January

2015-2016

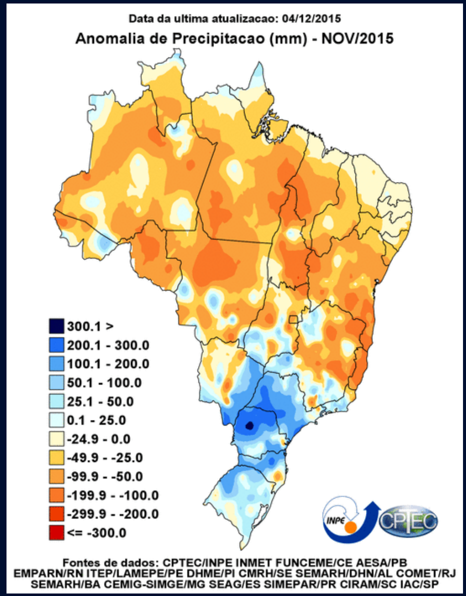

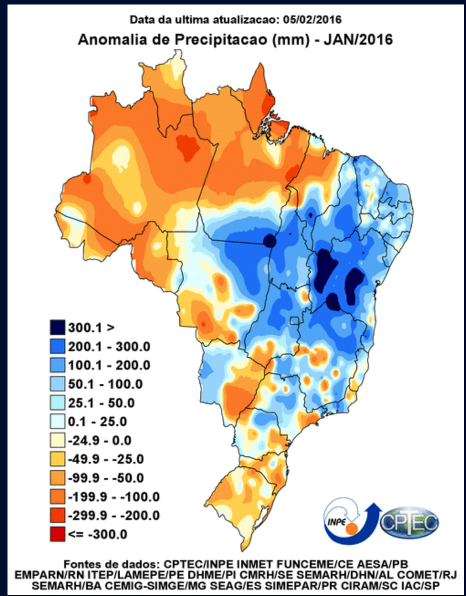

The intraseasonal variability, might be favored or hampered, according to its phase, by local circulation anomaly set up by processes triggered by conditions in spring, so that the first mode of interannual variability of summer precipitation is not just the rectification of intraseasonal variability or product of random sampling of intraseasonal events.

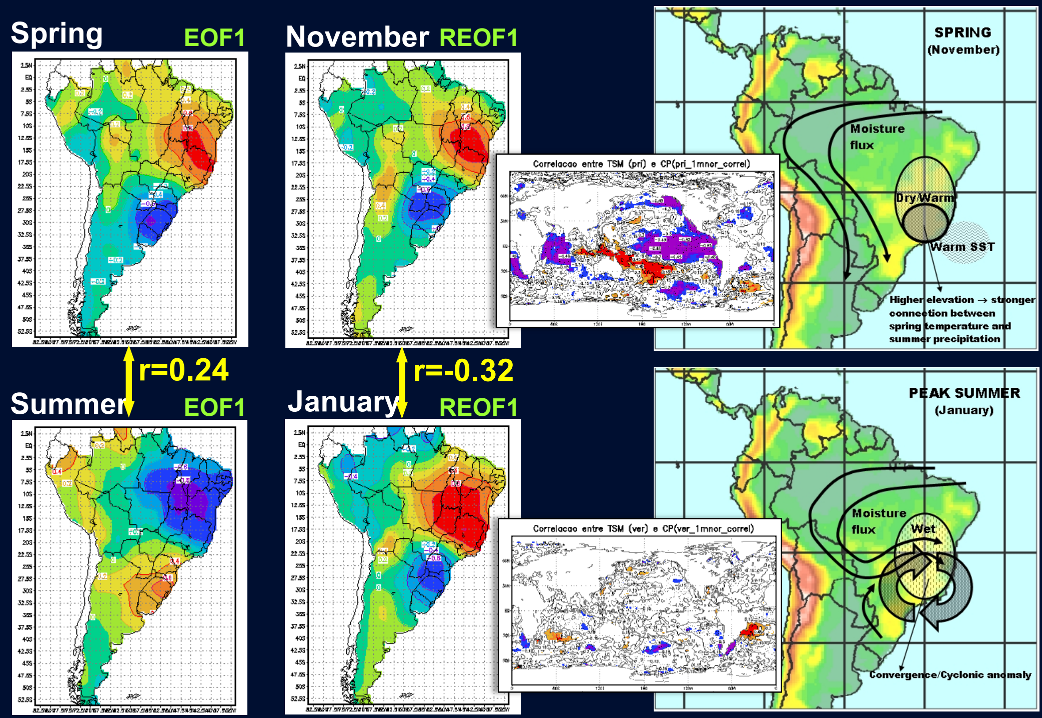

Grimm et al. 2007; Grimm and Zilli 2008

Evolution of the precipitation in Central-East Brazil

Do the models show the relationship between rainfall in spring and peak summer?

Outputs of the CPTEC/COLA AGCM seasonal simulations for the SMIP2 project are used in the analysis. This model was integrated with T62L28 resolution for the SMIP2 period (1979 to 2001), applying observed SST as boundary conditions. The model is run each year for four overlapping seasons, considering simulations of six months. In this study, the ensemble mean of five simulations for SONDJF is analyzed.

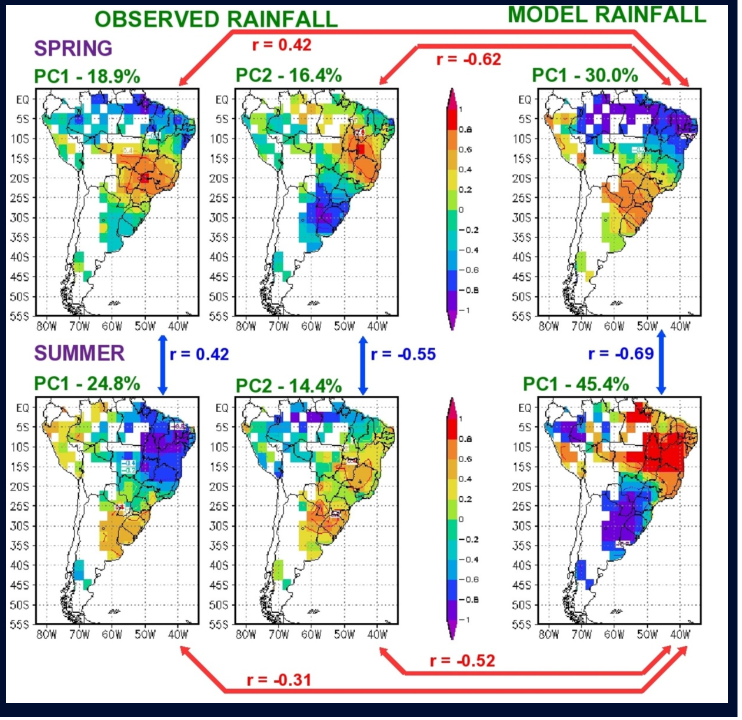

Models' skill in predicting monsoon rainfall (DJF)

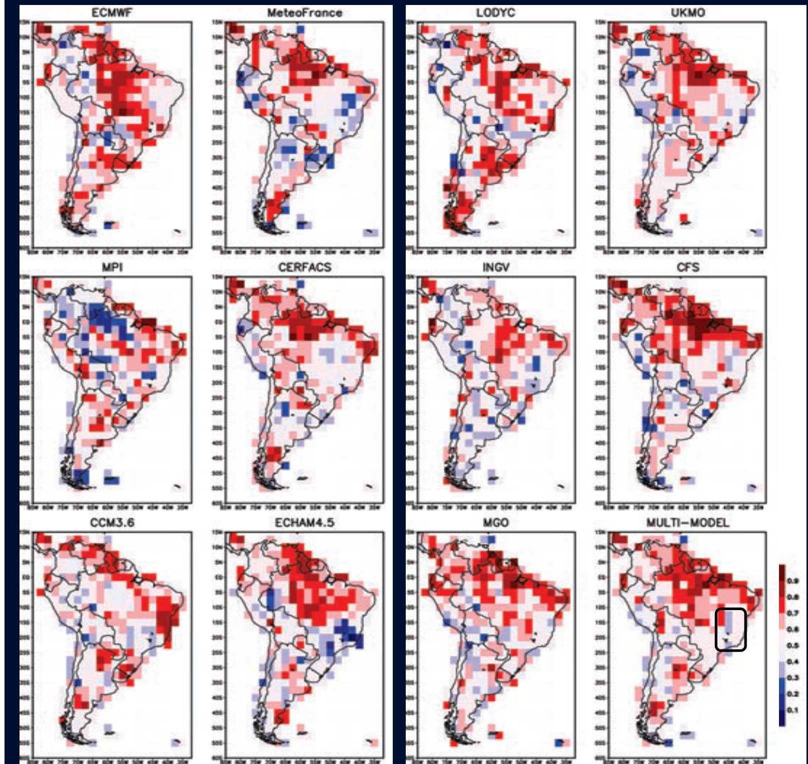

ROC (Cavalcanti et al. 2006)

Interdecadal variability

Interdecadal Variability

Spring

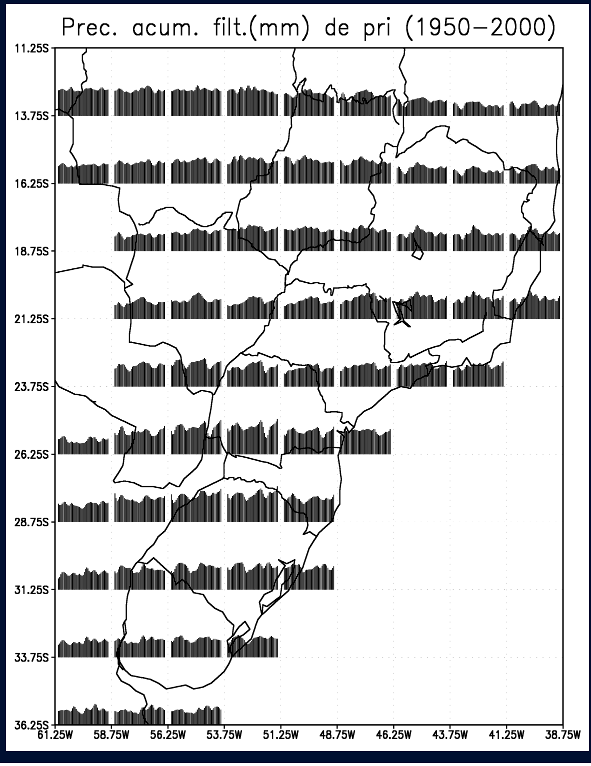

Summer

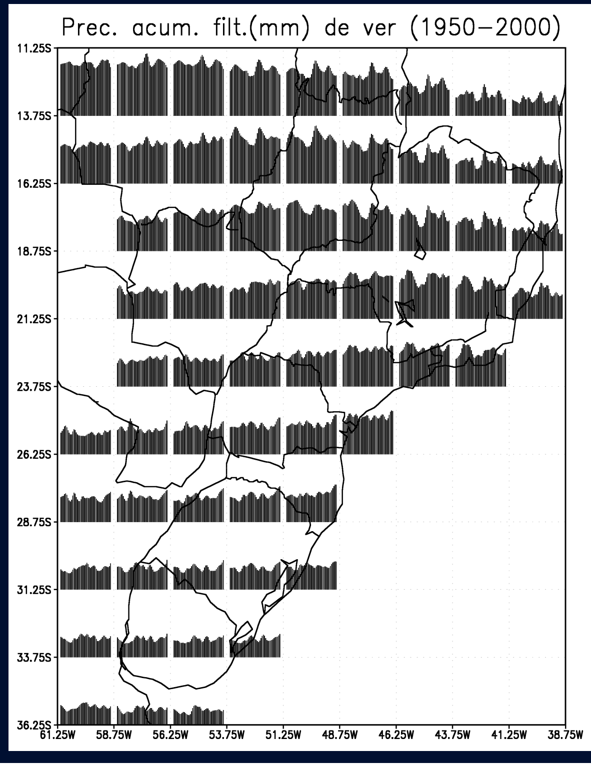

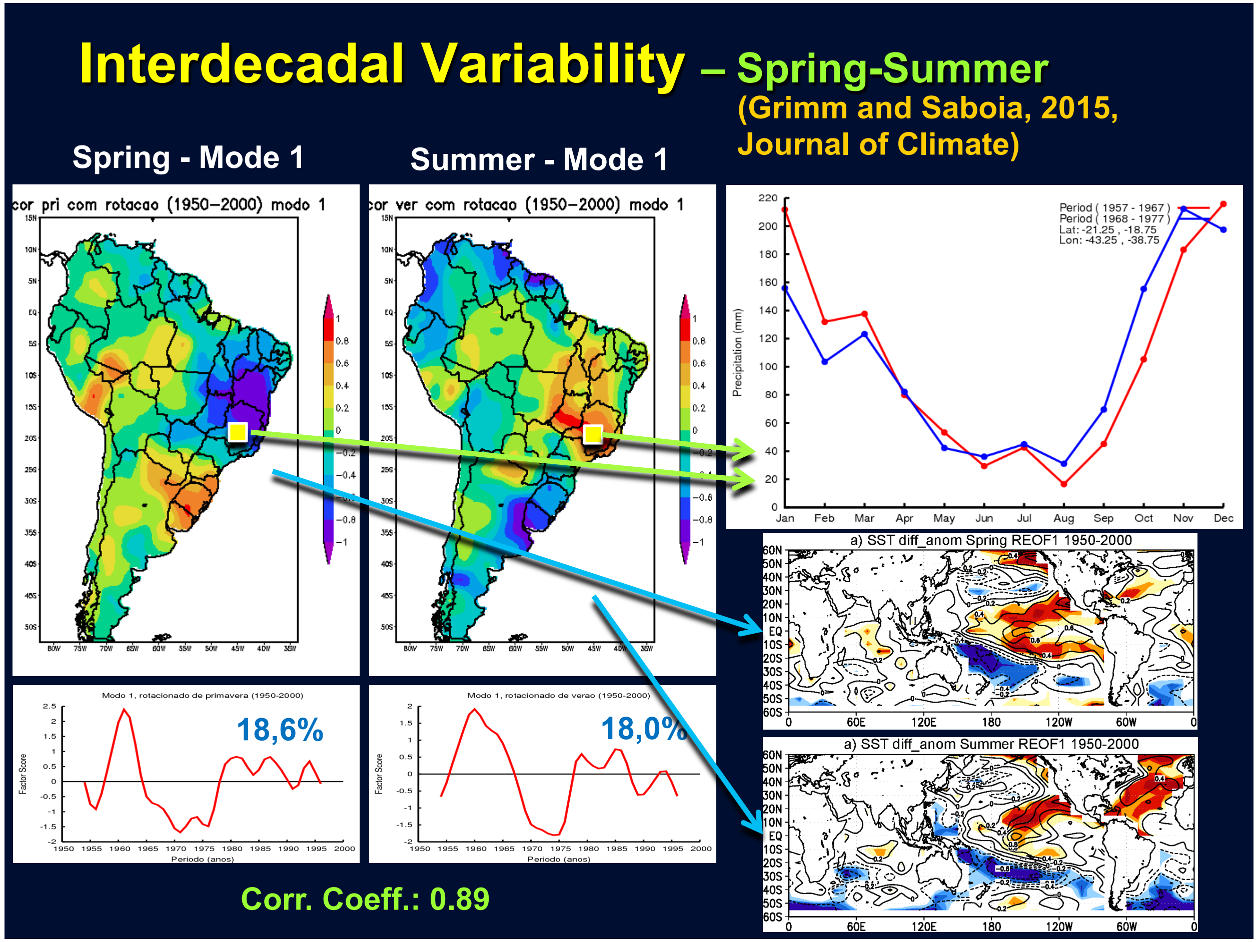

Interdecadal Variability – Spring-Summer
(Grimm and Saboia, 2015, Journal of Climate)
Spring - Mode 1
Summer - Mode 1
cor pri com rotacao (1950–2000) modo 1
cor ver com rotacao (1950–2000) modo 1
Period (1957 - 1967)
Period (1968 - 1977)
Lat: -21.25 , -18.75
Lon: -43.25 , -38.75
Precipitation (mm)
Jan Feb Mar Apr May Jun Jul Aug Sep Oct Nov Dec
a) SST diff_anom Spring REOF1 1950-2000
a) SST diff_anom Summer REOF1 1950-2000
Modo 1, rotacionado de primavera (1950-2000)
Modo 1, rotacionado de verao (1950-2000)
18,6%
18,0%
Factor Score
Periodo (anos)
Corr. Coeff.: 0.89

Interdecadal Variability: SST X precipitation

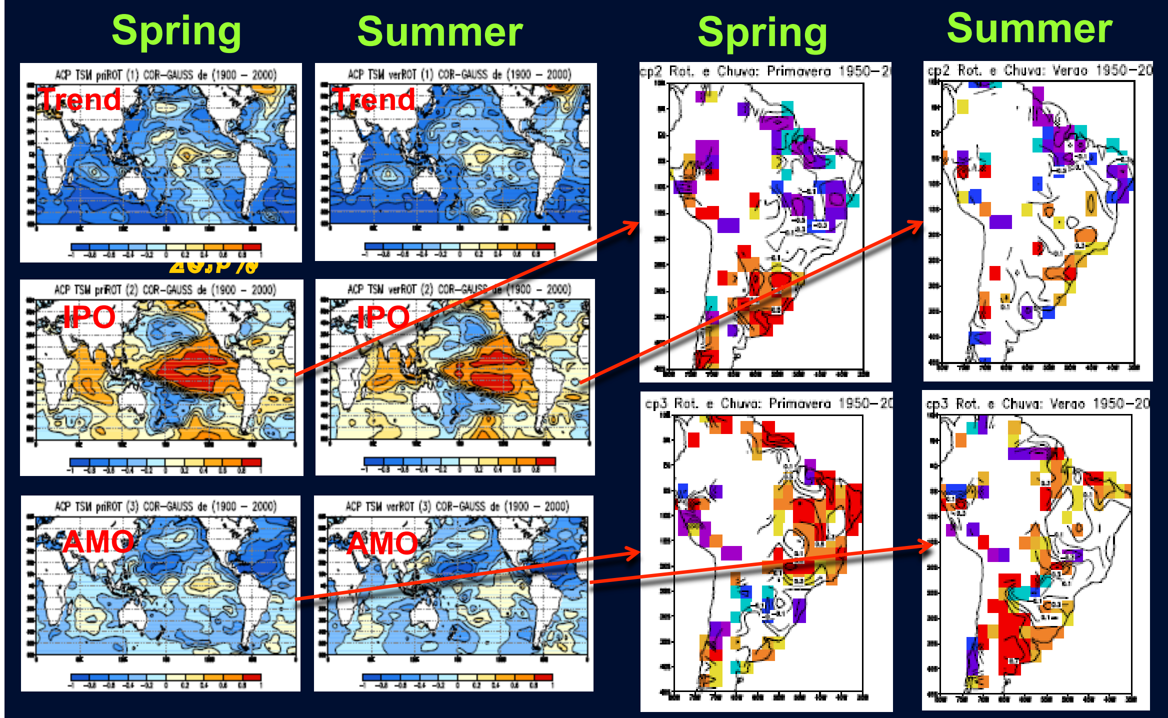

Summer - How changes the daily precipitation?

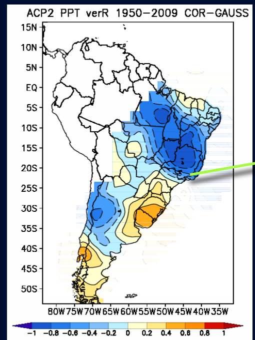

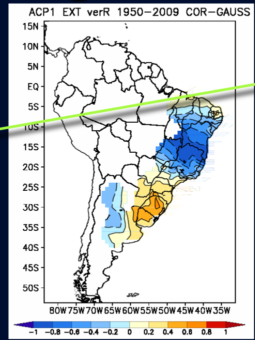

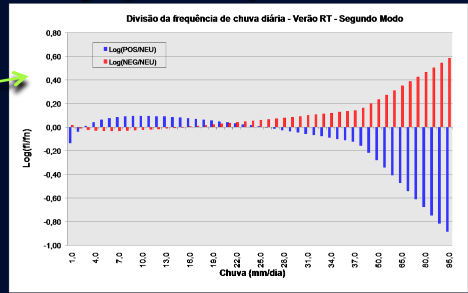

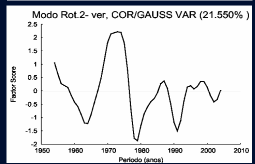

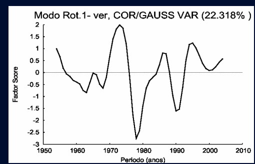

Logarithm of the frequency ratio positive/neutral (blue bars) and negative/neutral (red bars).

(Grimm and Saboia, 2016, Climate Research)

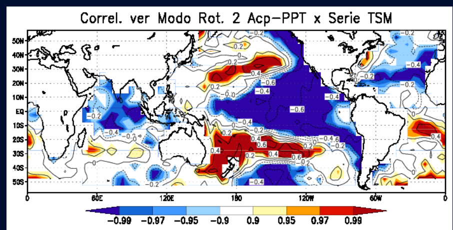

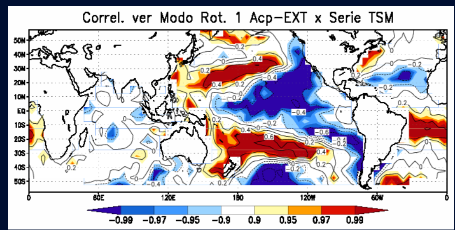

2nd interdecadal mode of precipitation and its correlation with SST

1st interdecadal mode of the frequency of extreme events and its correlation with SST